# Zeolite Synthesis and Its Application as a Separator

# For Safe Li-ion and Li-metal Batteries

by

Ramasai Dharani Harika Nalam

A Thesis Presented in Partial Fulfillment
of the Requirements for the Degree
Master of Science

Approved October 2023 by the
Graduate Supervisory Committee:

Jerry Lin, Chair
Heather Emady
S. Eileen Seo

ARIZONA STATE UNIVERSITY

December 2023

# ABSTRACT

Lithium-ion and lithium-metal batteries represent a predominant energy storage solution with the potential to address the impending global energy crisis arising from limited non-renewable resources. However, these batteries face significant safety challenges that hinder their commercialization. The conventional polymeric separators and electrolytes have poor thermal stability and fireproof properties making them prone to thermal runaway that causes fire hazards and explosions when the battery is subjected to extreme operating conditions. To address this issue, various materials have been investigated for their use as separators. However, polymeric, and pure inorganic material-based separators have a trade-off between safety and electrochemical performance. This is where zeolites emerge as a promising solution, offering favorable thermal and electrochemical characteristics. The zeolites are coated onto the cathode as a separator using the scalable blade coating method. These separators are non-flammable with high thermal stability and electrolyte wettability. Furthermore, the presence of intracrystalline pores helps in homogenizing the Li-ion flux at anode resulting in improved electrochemical performance.

This research delves into the preparation of zeolite separators using a commercial zeolite and lab-scale zeolite to study their safety and electrochemical performance in lithium-ion batteries. At low C-rates, both zeolites exhibited excellent capacity retention and capacity density displaying their potential to advance high-performance safe lithium-ion batteries. The commercial zeolite has demonstrated remarkable capacity retention and good

performance in terms of charge and discharge cycles, as well as stability. This makes it a valuable resource for the scaling up of electrode-coated separator technology.

Furthermore, the previous study demonstrated superior electrochemical performance of plate silicalite separator (also a lab-made zeolite) with both lithium-ion and lithium-metal batteries. However, the process of scaling up and achieving precise control over plate silicalite particle size, and morphology using the existing synthesis procedure has proven challenging. Thus, the modification of process conditions is studied to enhance control over particle size, aspect ratio, and yield to facilitate a more efficient scaling-up process. Incorporation of stirring during the crystallization phase enhanced yield and uniformity of particle size. Also, the increase in temperature and time of crystallization enlarged the particles but did not show any significant improvement in the aspect ratio of the particles.

Dedicated to

Venkata Vamsi Krishna Potla

Sai Siva Nageswara Rao Nalam

# ACKNOWLEDGEMENTS

Firstly, I want to express my heartfelt gratitude to my advisor, Dr. Jerry Lin for his unwavering guidance and mentorship throughout my academic journey. I am very grateful to him for trusting me and providing the valuable opportunity to work in his lab and project which ultimately enabled me to complete my thesis. His clarity of vision, wealth of experience and extensive knowledge have consistently inspired me, showing the right path and ignited my zeal to learn and thrive for excellence. I am immensely fortunate to have him as my mentor. He imparted numerous valuable lessons, from the art of designing initial experiments to understanding the profound meaning of results obtained.

I also extend my sincere appreciation to Dr. Heather Emady and Dr. Eileen Seo for graciously agreeing to serve as members of my committee.

I would like to thank my lab members, including Jose Lopez, Ayesha Rehman, Fateme Banihashemi, Dr. Lance and Mahsa Sharafi for all their support and help during my tenure in the lab. I would also like to thank Fred for being so helpful in fixing all the mechanical issues that occurred in the lab.

Finally, I wish to acknowledge the pivotal role played by my parents, sister, and my friend Dinesh in motivating me to pursue this degree. Their support and guidance have consistently empowered and encouraged me to face the challenges that life presents.

TABLE OF CONTENTS

PAGE

CHAPTER PAGE

APPENDIX PAGE

LIST OF TABLES

LIST OF FIGURES

Figure Page

Figure Page

Figure Page

# CHAPTER 1

# INTRODUCTION

## 1.1 Overview

In the present day, a significant portion of the electricity generated, and transportation utilizes non-renewable fossil fuels, giving rise to environmental issues such as global warming by $CO_2$ emissions. To mitigate the use of fossil fuels and safeguard the future world from energy crises and environmental problems, it is highly recommended to prioritize renewable and clean sources of energy such as solar, wind, and geothermal power. However, many renewable energy sources are affected by factors such as season and location. So, it is highly necessary that the excess energy produced needs to be stored[1,2]. Lithium-ion batteries (LIBs) represent the cutting-edge technology for a wide range of energy storage applications because of their exceptional traits such as high energy density, power density, long cycle life, and self-discharging nature[3].

Over the past few years, the market has been driven by the trend of making electronic devices smaller, which increased the demand for portable power resources significantly. In certain instances, the battery system contributes to half of the weight and volume of the device it powers. Hence, there is a serious requirement to reduce the overall weight and space occupied by the battery system in electronic devices. For this purpose, Lithium batteries could be chosen as they offer lightweight, high voltage, and greatest energy density[4]. The initial documented interest in lithium batteries was sparked by the research conducted by Harris in 1958[5]. Eventually, the commercialization of primary lithium-ion

batteries began during the 1970s when the first rechargeable battery was suggested by M.S. Whittingham, while he was working at Exxon in 1976[1][4].

Secondary lithium-ion batteries have energy density ranging between 250-680 $W/m^3$ and specific energy of 100-270 Wh/Kg which is very high and advantageous for power-efficient electronic devices[6][7]. Among all the metals, lithium is the lightest and has the greatest electrochemical potential, also offers high specific energy per weight (3860 mAh/g). In fact, Lithium batteries with Li metal as anode (Lithium-metal batteries) provide exceptionally high energy densities compared to lithium-ion batteries. However, LMBs have certain safety concerns such as internal short-circuiting due to the propagation of lithium dendrites which can cause thermal runaway[8].

**1.2 Elementary concepts**

Lithium-ion batteries consist of two electrochemically active electrodes (anode and cathode) coated on two different current collectors (copper and aluminum, respectively), a separator that is electrochemically inactive and sandwiched between the two electrodes, and the electrolyte, which is a medium for the transfer of ions. The separator does not take part in the electrochemical reactions that occur inside the cell. However, it still renders the critical functions of separating the two electrodes to prevent internal short circuit and facilitates the movement of lithium ions through its pores [9].

The extensively used cathode materials are lithium metal oxides such as lithium cobalt oxide (LCO), lithium manganese oxide (LMO), lithium titanium oxide (LTO), and lithium manganese nickel cobalt oxide (NCM) whereas graphite is the most commonly used anode[10]. During the process of charge and discharge, these cathode materials release

lithium ions due to the change in their crystal lattice. The separator is porous in nature. It helps in the transfer of lithium ions between the electrodes and hence should offer minimum internal resistance. It should also be highly wettable and have high electrolyte uptake for better performance. The most frequently used electrolytes are liquids which have lithium salts dissolved in carbonate solvents such as Ethyl Carbonate (EC), Dimethyl Carbonate (DMC), and Diethyl Carbonate (DEC) in different ratios[11][12]. The salt dissociates in the solvent to improve the lithium-ion conductivity and the solvent solvates the lithium-ions from salt and electrodes to support their transfer[13].

In the battery literature terminology, the anode is lithium-ion acceptor, and the cathode is lithium-ion donor during the charging process. While charging, a battery is connected to an external voltage source, creating an electric potential difference. This results in the transfer of Li-ions from the cathode to the anode through the electrolyte. To balance this ion transfer, electrons from the cathode travel to the anode in the external circuit. During the process of discharge, lithium-ions stored at the anode travel back to the cathode, and the electrons move from the anode to the cathode in the external circuit, making the electric current. The discharging of lithium-ion batteries is a spontaneous process [14]. Figure 1.1 illustrates the ion and electron transfer during the charging and discharging processes in a Li-ion battery:

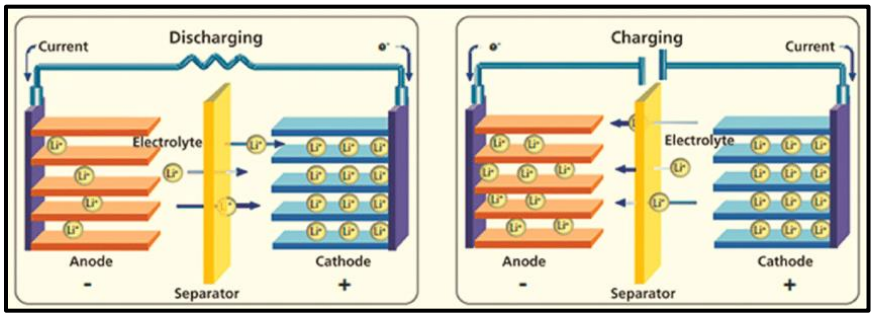

Fig 1.1 Pictorial representation of charging and discharging cycles between anode and cathode in a Li-ion battery[15]

### 1.3 Literature review

Lithium-ion batteries take the lead in energy storage due to their exceptionally high capacity and energy density. Despite having numerous advantages, there are certain safety concerns associated with lithium-ion batteries that pose a serious threat to the life surrounding them. We know that these batteries are composed of highly reactive materials that can ignite and react vigorously if they come into contact with the atmosphere. There have been numerous prominent fire and explosion accidents that have raised public concern for the risks associated with lithium battery fires[16].

The safety performance of these batteries is compromised by the use of low thermal stability electrodes and separator materials. The primary safety concern that restricts their application in large-scale operations is thermal runaway (TR), a process that can cause fire and explosion which creates a life-threatening situation. Furthermore, it can lead to the release of toxic gases such as CO, HF, and other fluorine-containing gases due to the combustion of the battery components during the process, which can further worsen the situation[17][18].

A series of exothermic reactions occur within the battery when it is exposed to abusing conditions or extreme operating conditions, which in turn produces more heat that can quicken the reaction kinetics. The release of enormous amounts of heat due to the thermal runaway causes a fire, and the toxic gases liberated inside the battery build up large amounts of pressure, which causes an explosion. The primary reason for the occurrence of

the thermal runaway is subjecting the battery to extreme operating conditions that include electrical (Overcharging and discharging), mechanical (crushing), and thermal (overheating) abuse conditions[19][20].

Overheating of the battery usually happens when there are some loose connections between the cells in the pack, which leads to an external short circuit and results in local overheating. The electrical abuse of batteries could be observed when there is the failure of the battery management system (BMS), due to which overcharging and discharging of the battery happens and results in the internal short circuit. Crushing and metal penetration into batteries happen in case of accidents that can potentially damage battery components and lead to internal short circuit[20].

The internal components of the battery decompose as the temperature increases. The separator breaks down at temperatures between 130-170℃ and the electrolyte decomposes at 120℃. The decomposition of the SEI layer on the anode occurs at 100℃. During the thermal runaway, both the electrodes react with the electrolyte and release oxygen, which increases the risk of causing fire. $LiPF_6$ dissolved in carbonate solvents (DEC/DMC/EC) is one of the conventional electrolytes popularly used. During TR, the $LiPF_6$ salt decomposes and releases HF on further reaction. The complete and partial oxidation of carbonate solvents occurs, releasing carbon dioxide and carbon monoxide gases. Thus, the quantity of electrolytes present in the battery can impact the overall heat production of the entire cell during thermal runaway[21].

$$LiPF_6 \leftrightarrow LiF + PF_5$$

$$2.5\ O_2 + C_3H_4O_3\ (EC) \rightarrow 3\ CO_2 + 2\ H_2O$$

$$6\ O_2 + C_5H_{10}O_2\ (DEC) \rightarrow 5\ CO_2 + 5\ H_2O$$

$$3\ O_2 + C_3H_6O_3\ (DMC) \rightarrow 3\ CO_2 + 3\ H_2O$$

Complete Oxidation

$$O_2 + C_3H_4O_3\ (EC) \rightarrow 3\ CO + 2\ H_2O$$

$$3.5\ O_2 + C_5H_{10}O_2\ (DEC) \rightarrow 5\ CO + 5\ H_2O$$

$$1.5\ O_2 + C_3H_6O_3\ (DMC) \rightarrow 3\ CO + 3\ H_2O$$

Partial Oxidation

Therefore, to develop safe lithium-ion batteries, it is important that thermal runaway is prevented even if the battery is subjected to abuse/extreme operating conditions such as short circuit, overcharging, and nail penetration.

**1.4 Limitations of the conventional polymeric separators**

The separator is a supercritical component in the battery system as it plays an important role in separating the anode and cathode. As mentioned earlier, it is electrochemically inactive, and its thickness ranges between 20-30 μm[22]. The characteristics that make a separator ideal are low ionic resistance, high thermal and mechanical stability, electrolyte wettability and uptake, chemical inertness towards the other components in the battery, and scalable manufacturing. The traditional separators used in lithium-ion batteries are polymeric in nature (polypropylene (PP), polyethylene (PE)). These polymeric separators are not usually highly wettable and mechanically stable. They suffer a huge dimensional shrinkage at high temperatures (usually temperatures higher than 135 ℃) resulting in internal short circuit that can trigger thermal runaway[23]. Therefore, there is a need to

create non-flammable separators that are both electrochemically and mechanically stable and durable to achieve improved safety performance.

Various research groups tried improving the safety performance of the polymeric separators by embedding inorganic materials in or onto them. Thus, inorganic materials are added either by coating them on the polymeric separators or by incorporating them into the polymeric separator matrix[24]. Polyethylene separator is usually coated with $Al_2O_3$ and polydopamine to improve its thermal stability and electrolyte wettability[25]. The various coating methods used for this purpose are dip coating, atomic layer deposition, and sol-gel technique[26][27]. Though these coated separators are thermally stable compared to pure polymeric separators, they are yet not completely safe as the major portion of the separator is still polymeric. Another approach to adding inorganic materials to the separator is incorporating them into the polymer matrix. However, the bulk being polymeric, they are not thermally stable leaving room for failure. They also do not have good electrolyte wettability and uptake[28]. The most efficient way to make non-flammable and thermally stable separators is to completely eliminate polymeric materials and use only inorganic materials in them.

Pure inorganic materials (ceramics) such as alumina and silica, which are hydrophilic, have excellent thermal stability and electrolyte wettability. But the free-standing separators made out of pure inorganic materials are extremely fragile and exhibit poor flexibility with the cell winding assembly[29]. To make them robust, there is a need to increase the thickness to 200 μm, which increases the internal resistance of the cell and results in poor performance[30]. However, it also needs a large amount of binder, and the synthesis

procedure is complicated, intensive. Hence, to make sturdy inorganic material-based separators with lower thickness, another approach is necessary.

Lately, a new approach of coating the inorganic materials using an organic binder onto the electrodes has been reported in the literature by Dr. Lin's group. The procedure is scalable, easy, and cost effective. In this approach, a slurry is made by mixing the inorganic materials ($Al_2O_3$ and $SiO_2$) with an organic binder, PVA, and the solvent, water. The uniform slurry is then coated onto the electrode using a doctor blade and vacuum dried to obtain a polymer-free inorganic separator. The thickness of the coated separator can be controlled using the doctor blade. Usually, a 40 µm thick coating is made onto the cathode of 60 µm thickness. They have exhibited high thermal stability, good electrochemical performance, better mechanical stability, and the synthesis is scalable. Despite of its numerous advantages, the overall weight of the battery is increased due to the high density of particles, resulting in reduced weight-based energy density. Also, as the separator's metal oxide particles are dense, lithium-ion transport exclusively takes place through inter-particle pores. This results in uneven distribution of lithium ions at anode giving rise to hotspots and non-uniform SEI formation[31][32].

To address these limitations of pure silica and alumina separators, zeolites are studied. Zeolites are 3-d aluminosilicate frameworks with less density compared to $SiO_2$ and $Al_2O_3$ and possess intraparticle pores. These pores help in the even distribution of Li-ion flux at the anode and facilitate the formation of stable SEI[31]. In this context, pure silica-based MFI type zeolites called silicalites exhibited promising results in terms of safety as well as electrochemical performance.

Previously from our research group, Kishen has reported the use of pure silica-based zeolite-coated separators (silicalite separators), which are highly wettable and non-flammable. The study compared the performance of lab-scale zeolite with pure silica ($SiO_2$) and PP separators with a fire-proof and high concentrated electrolyte[31]. The findings of the study concludes that the lab-scale zeolite separator, owing to its superior wettability, facilitates more uniform electrolyte access to the anode and the anode-separator interface. This leads to the formation of a uniform solid-electrolyte interface (SEI) at the anode surface. Consequently, the SEI thus developed is thin and robust in comparison to the pure silica and polymer separators, resulting in reduced SEI and charge transfer resistance.

Later, Dheeraj and et.al studied the impact of the morphology of silicalite particles on the electrochemical performance of the battery. For that purpose, he utilized two MFI-type silicalites. They are 1. lab-scale zeolite and 2. plate silicalite[33]. The results of the study suggested that plate shaped silicalite separator has demonstrated superior capacity retention and rate capability while exhibiting lower SEI and charge transfer resistance compared to the lab-scale zeolite. This enhancement of electrochemical performance is attributed to the more uniform Li-ion flux through the intraparticle pores along with interparticle pores at the separator-anode interface.

**1.5 Research Objective**

Lab-scale zeolite and plate silicalite are synthetic pure silica MFI type zeolites (silicalites) made in the laboratory using hydrothermal synthesis under stagnant conditions. The yield of this process is very low, which is around 35-40%. For commercializing electrode-coated silicalite separators, the acquisition of substantial quantities of silicalite for cathode coating

and subsequent electrochemical testing is paramount which means the scaling up of silicalite synthesis is indispensable. However, with the given yield of the hydrothermal synthesis, it takes a significant amount of time to make the required amount of silicalite which is not feasible to design and execute experiments within the specified timeline.

Moreover, the scaling up also encounters various challenges due to the use of stagnant conditions during the crystallization phase. The absence of agitation of the solution during the hydrothermal synthesis results in poor control over the particle size and aspect ratio. All these limitations associated with the lab made silicalite, encouraged me to explore a commercial MFI type zeolite that is pure silica-based with similar particle size as that of lab-made silicalite and make coin cells for performance comparison against silicalite-based counterparts.

### 1.6 Thesis Structure

The first chapter of my thesis primarily focuses on the study of the performance of a commercially purchased MFI zeolite (pure silica-based) and the zeolite (lab-scale zeolite) synthesized in the lab as separators. Both the commercially purchased and lab-scale zeolites are coated onto the cathode, and coin cells are made using the electrolyte, 1M $LiPF_6$ in 1:1:1 (v/v/v) in EC/DEC/DMC. Subsequently, the cells are tested for their charge-discharge performance, impedance parameters, and long-term cycle life. The cathode used for this study is NCM (5:3:2, from MTI) and the anode used is graphite (from MTI). Also, various characterization techniques are used to analyze the zeolite powders and free-standing separators. Scanning Electron Microscopy (SEM), X-ray Diffraction (XRD) and Fourier- Transform Infrared Spectrum (FTIR) are the techniques used to characterize both

the powders and separators to gain more insights into the particle shape, size, orientation, and chemical bonds present in the zeolite powders. To evaluate the wettability and thermal stability of the separators, the contact angle method, thermo gravimetry analysis and differential scanning calorimetry (TGA-DSC) are used.

The previous study by Dheeraj et al.[33], demonstrated the superior rate capability and capacity retention of the plate silicalite separator with fireproof high viscous electrolyte.

However, as discussed earlier, the synthesis procedure of plate silicalite face scaling up, yield and process control issues due to the crystallization occurring under stagnant conditions. Thus, the second chapter of my thesis focuses on modifying these process conditions to obtain enhanced yield and precise control over the particle size to scale up the synthesis effectively.

This can be achieved by varying the precursor quantities in the seeding solution, adjusting the temperature, time, and use of agitation in the hydrothermal synthesis. The sole aim in doing so is to obtain a substantial yield of high aspect ratio coffin shaped/plate shaped MFI type zeolite particles. The high aspect ratio is very useful when the plate silicalite is coated as a separator onto the cathode because it effectively prevents the propagation of lithium dendrites by forming a robust, mechanically stable, and highly tortuous.

# CHAPTER 2

# STUDY ON THE PERFORMANCE OF LITHIUM-ION BATTERIES UTILIZING ZEOLITE-COATED SEPARATORS

## 2.1 Introduction

Zeolites were initially identified in sediment and pegmatite rocks. Natural zeolites find their primary applications in water treatment, agriculture, and soil remediation. Their synthetic counterparts have a wide range of industrial uses. Molecular sieving and heterogeneous catalysis are the major industrial applications of synthetic zeolites. They are known for their remarkable adsorption and ion exchange properties[34].

Zeolites are three-dimensional crystalline frameworks consisting of tetrahedral units composed of silicon, aluminum, and oxygen atoms. These structures create channels that have well-defined sizes and shapes. However, for the applications in lithium-ion batteries, we need hydrophobic, thermally stable, highly wettable, and less dense materials. Silicates are microporous crystalline structures that have all the required ideal characteristics such as chemical stability, high wettability, and thermal strength[35][36].

Therefore, silicalites are studied for their use as separators in lithium-ion batteries. As outlined in the research motivation, silicalite synthesis process encounters numerous challenges when it comes to scaling up. Hence, a commercial zeolite is procured and evaluated for its performance as a separator in comparison with the lab-scale zeolite in the context of commercialization of electrode coated zeolite separators.

Both of these zeolites are MFI type zeolites with a particle size of 2-3 µm and spherical, plate morphology. They are effectively coated onto the cathode (NMC) as separators, and

the electrochemical characteristics of the coin cells are tested. The results demonstrate their superior performance over the coin cells with polypropylene (PP) as a separator. This section of study delves into a comprehensive evaluation of the performance of these zeolite-coated separators.

## 2.2 Experiment

### 2.2.1 Determination of interparticle porosity of zeolites

Lab-scale zeolite and the commercial zeolite are MFI type zeolites with a porosity of 80% and 72% respectively. The lab-scale zeolite has a crystal density of 1.76 g/cc[31]. The interparticle porosity of these zeolites is measured by using the tapping method. To determine the porosity, some specified amount of powder is taken and subsequently transferred into a graduated cylinder. The bulk volume of the powder is recorded. The graduated cylinder is then tapped until no further reduction in the volume is seen, and that volume is recorded as actual volume. To derive the porosity value, both bulk and actual densities are computed using the following formulae:

$$\rho_{bulk} = \frac{\text{Mass of the sample}}{\text{Bulk volume of the sample}}, \rho_{actual} = \frac{\text{Mass of the sample}}{\text{Actual volume of the sample}}$$

$$\text{Porosity} = 1 - \frac{\rho_{bulk}}{\rho_{actual}}$$

However, powder porosity is different from the porosity of coated separators. The porosity of coated separators can be calculated using the following equation:

$$R = \frac{d}{k \times A \times \emptyset} \quad (2.1)$$

Where,

d = thickness of the separator

A = crossectional area of the separator

K = conductivity of the separator

∅ = porosity of the separator

### 2.2.2 Synthesis of lab-scale zeolite

The synthesis of lab-scale zeolite involves the utilization of three primary precursors: tetraethyl orthosilicate (TEOS, reagent grade, 98% procured from Sigma Aldrich), TetrapropylAmmoniumhydroxide (1.0M in $H_2O$, TPAOH solution from Sigma Aldrich) and deionized water (DI) water. TEOS serves as the primary source of silica in the solution, while TPAOH acts as the organic template. Initially, 12 g of TPAOH is added to 202 grams of DI water, followed by the addition of 10 grams of TEOS while stirring solution. The beaker is sealed with a paraffin wax film to avoid evaporation losses. The entire solution is stirred for 24 hrs at room temperature to obtain a clear solution.

Subsequently, the solution is divided into two 100 ml autoclaves and the autoclaves are placed in the oven which is preheated to 130 ℃. The solution filled autoclaves are heated for 8hrs to obtain a plate shape morphology with a particle size of 2 µm.

After the hydrothermal synthesis, mother liquor is drained to collect the silicalite crystals. The crystals are then washed with DI water and centrifuged at 10,000 rpm for 20 mins. This process of washing and centrifugation is repeated 3 times to ensure the complete removal of any remaining organic materials from the reaction. After 3 times of washing and centrifugation, the crystals are washed again, and then the solution is dried at 100 ℃ for 24 hrs. During drying, all the water content is evaporated, and powder remains in the beaker. The powder is meticulously grinded using a motor and pestle before the final step to break any potential aggregates that are present.

The final step involves the calcination of powder ,where the powder is heated to 600 ℃ for 10 hours to remove the organic template. This synthesis procedure has been adopted from the literature[31][37].

### 2.2.3 Coating and making of zeolite separators

To coat the zeolites, slurries of the powders are made. Subsequently, the slurries are coated as separators onto the cathode material, NCM. For lab-scale zeolite, the slurry is made by mixing 1 gram of powder with 1 gram of 5 wt% polyvinyl alcohol aqueous solution (PVA) and 0.5 grams of deionized (DI) water. The slurry of commercial zeolite is made by mixing 2.5 grams of powder with 0.5 grams of 5 wt% polyvinyl alcohol aqueous solution (PVA) and 2 grams of deionized (DI) water. The PVA content added to the slurry is reduced to a minimum level to mitigate its effect on the electrochemical performance of the cell and to improve thermal stability of the separator.

To make 5 wt% PVA aqueous solution, 5 grams of PVA (molecular weight: 77000-79000, from ICN Biomedical Inc, USA) is dissolved in 95 grams of DI water. The comprehensive procedure is to take a conical flask and add 95 grams of DI water to it. Subsequently, 5 grams of PVA powder is weighed and dissolved into the DI water while stirring. The solution is magnetically stirred for 24 hours until a clear solution is obtained. It is important to note that freshly made PVA is preferred while making a coating of the separator. However, the PVA aqueous solution remains effective for up to one month. After this period, the solution should be reprepared to ensure optimal results.

The slurry mixtures are gently stirred for about 10 mins using a glass stirrer to break down any aggregates that may be present in the mixture. This step is crucial to achieve a

consistent and homogeneous slurry while preventing the formation of any bubbles. Subsequently, the slurry is coated on to the NCM (typically 5inch×5inch) using a blade coater (Doctor blade, Gardco LLC, USA). To coat 40 µm thick separator, the height of the blade coater is adjusted accordingly from the base.

The prepared slurries (lab-scale zeolite, commercial zeolite) are dropped on one side of the cathode and spread along the length of the cathode to obtain a uniform coating, followed by drying in a humid chamber at 40 ℃ and 60% relative humidity for 8 hours. The electrode-coated separators are then cut into 16 mm discs using a cutting machine (MSK-T10 from MTI). This procedure may require some finesse to keep the separator crack free. The electrode-coated separator sheets are sandwiched between two weighing papers while cutting them. Later, the discs are activated in a vacuum oven by heating them at 70℃ for 12 hrs. This process serves the dual purpose of activating the cathode and removing the traces of moisture, if any present. Following activation, the electrode-coated discs are transferred carefully into the glove box for the preparation of coin cell assembly.

### 2.2.4 Characterization of zeolite separators

The morphology and cross-sectional characteristics of the zeolite separators are observed using Scanning Electron Microscope (SEM, focused ion beam – Auriga – Zesis). X-ray Diffraction patterns (XRD, PANalytical aeris powder x-ray diffractometer) are generated for both the zeolite powders and separators to analyze the phase structure of the particles. Fourier - Transform Infrared Spectrum (FTIR, PerkinElmer Frontier FTIR) is utilized to identify the types of chemical bonds present in both the zeolite variants. Additionally, the

separators are tested for their wettability and thermal stability using contact angle (Kruss Easy drop goniometer) and TGA/DSC (Labsys Evo from Setaram) techniques respectively.

### 2.2.5 Coin cell construction and Electrochemical characterization

The coin cells made are CR2032 type which indicates the battery has 20mm diameter and 3.2mm thickness. The components used to make a coin cell include bottom case, stainless steel spacers, cathode, separator, electrolyte, anode, spring, and top case. All the components of the cell except for the cathode, anode, separator, and electrolyte are sourced from X2 Labwares, Singapore. It is important to note that constructing coin cells can be challenging and has potential to affect the results if not executed properly.

The cell construction begins with the bottom case. The bottom case is taken, followed by the placement of a spacer and then the separator-coated cathode with the coating facing up. Subsequently, 120 µL of electrolyte (1M $LiPF_6$ in EC/DEC/DMC in 1:1:1 v/v/v ratio) is measured and dropped onto the separator. The anode is then placed with the carbon surface facing towards the separator. Next, a spacer and a spring are placed on the top of the anode, and the cell is sealed using a top case. Finally, the arrangement is turned upside down and coin cell is crimped using the crimping machine (from MTI) at a pressure of 400 psi. As the coin cell is crimped, any excess electrolyte present inside comes out that is carefully cleaned and removed. Figure 2.1 shows the pictorial representation of coin cell assembly.

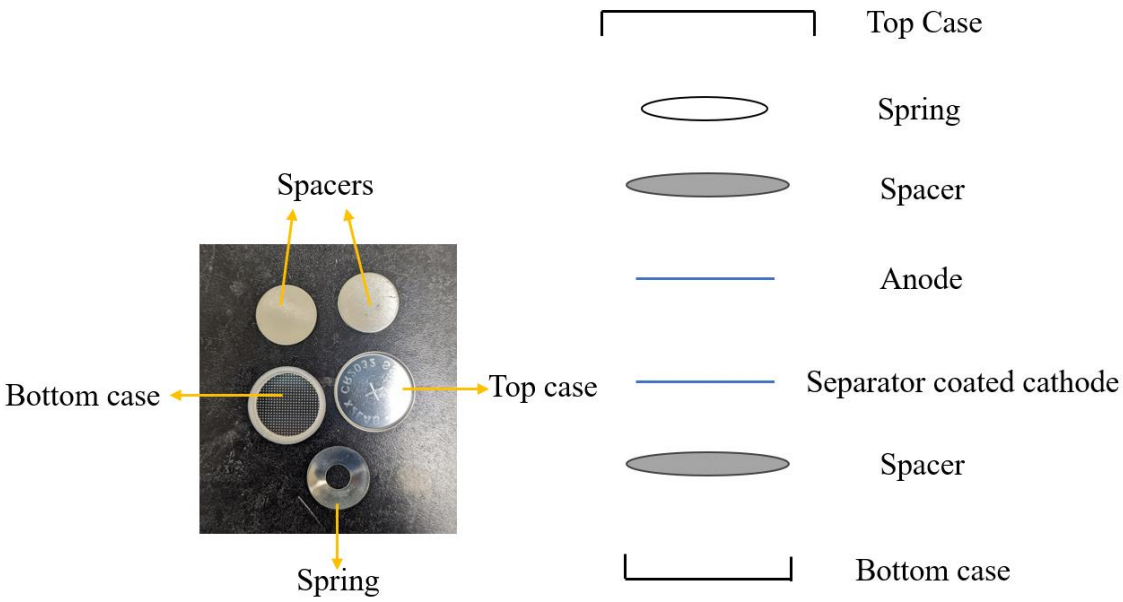


Fig 2.1 Coin cell components and assembly

The constructed coin cells are taken out of the glove box and tested for their charge-discharge characteristics. For this purpose, the equipment used is NEWARE battery testing system (BTS 3000 from Neware Co, Shenzhen, China). The coin cells are subjected to cycling using the CC-CV (constant current-constant voltage) method with voltage limits set at 3 V and 4.2 V.

The coin cells made with commercial zeolite and lab-scale zeolite separators are tested at 0.1C rate for 50 cycles to assess the cycle life performance of the cells. Additionally, Electrochemical Impedance Spectroscopy (EIS) is employed to the coin cells using the PARSTAT 2263 EIS station (Princeton applied research, USA) operating in AC mode to analyze different types of internal resistances in the cell. The frequency limits set for this measurement are 100 KHz and 1.5 Hz with an AC amplitude of 10 mV rms. Nyquist plots

generated are analyzed in EC lab to determine the internal resistances attributed by the separator, SEI, and ion-transfer.

## 2.3 Results and Discussion

### 2.3.1 Characterization of Powders and Coated Separators

Both the lab-scale zeolite and commercial zeolite exhibited remarkably consistent and smooth coating on NMC as shown in the Figures, 2.2(a) and 2.2(b). The smooth texture of the separators indicate effective particle packing of both zeolites when coated using a blade coater.

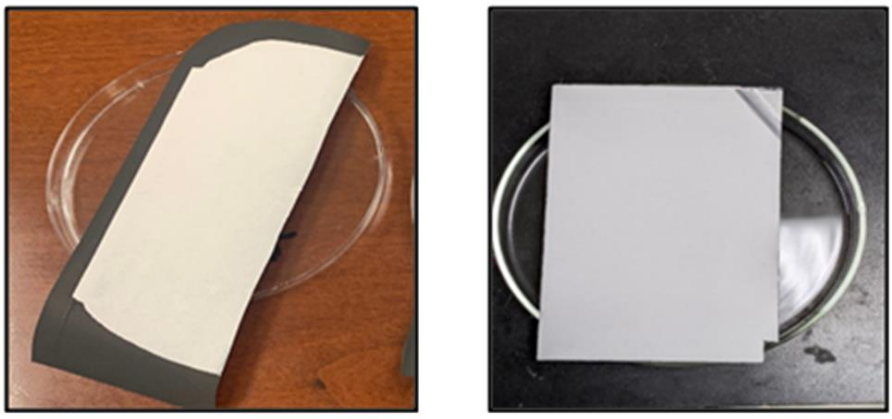

(a) (b)

Fig 2.2 Images of (a) Lab-scale zeolite and (b) Commercial zeolite coated onto the NCM after humid drying

The optical images of the electrode-coated separators are also captured to examine for any point defects, such as pin holes, formed due to the bubbles in the slurry. Figures 2.3(a) and 2.3(b) below show that the coatings of lab-scale zeolite and commercial zeolite are uniform and defect-free respectively.

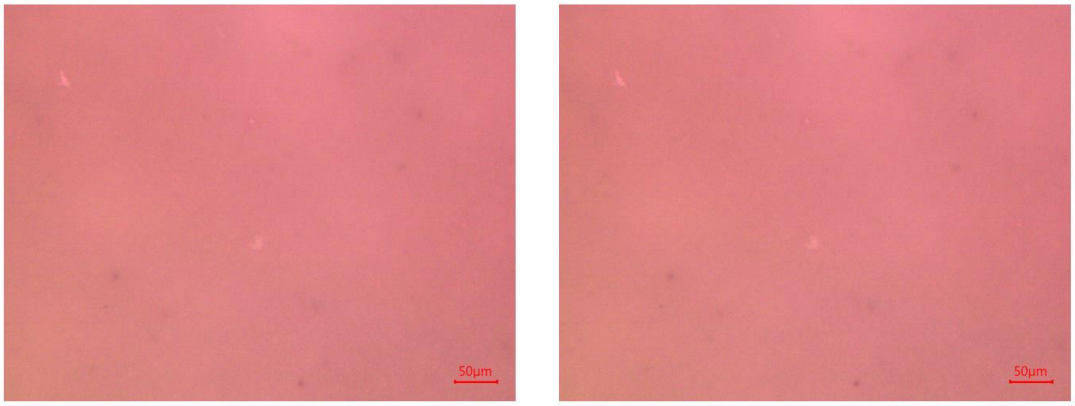


(a) (b)

Fig 2.3 Optical images of (a) lab-scale zeolite and (b) commercial zeolite coated on NMC

Scanning Electron Microscope (SEM) Imaging

The electrode-coated separators are viewed under SEM along with the powders to analyze shape, size, consistency of the particles, and thickness of the coating. The 40 µm thick separator is shrinked to around 30 µm after the process of drying.

The sample preparation procedure for both the zeolite-coated separators to view under SEM is the same. The main objective of this characterization technique is to examine the surface as well as the cross-sectional aspects of the separator. Thus, we have two types of imaging: 1. Surface imaging and 2. Cross-sectional imaging. The sample preparation process differs for each type of image.

For surface images, a small section of the electrode-coated separators is cut and affixed onto the SEM sample holder by means of a carbon tape. This allows us to observe the surface characteristics, such as particle shape and size with high precision. In contrast, for cross-sectional images, using scissors to cut, could potentially damage the cross-section of the separators and alter the cross-sectional thickness. To overcome this challenge, the

separators are immersed in liquid nitrogen for about 10 mins to freeze. Once they are frozen, a portion of the separators is broken using two clean tweezers, and they are mounted onto the SEM sample holder.

It is important to note that the sample holders used for surface imaging and crossectional imaging are also different to attain good quality images. Figures 2.4(a) and 2.4(b) show the samples prepared for surface imaging, while Figures 2.4(c) and 2.4(d) show the samples made for cross-sectional imaging before gold coating.

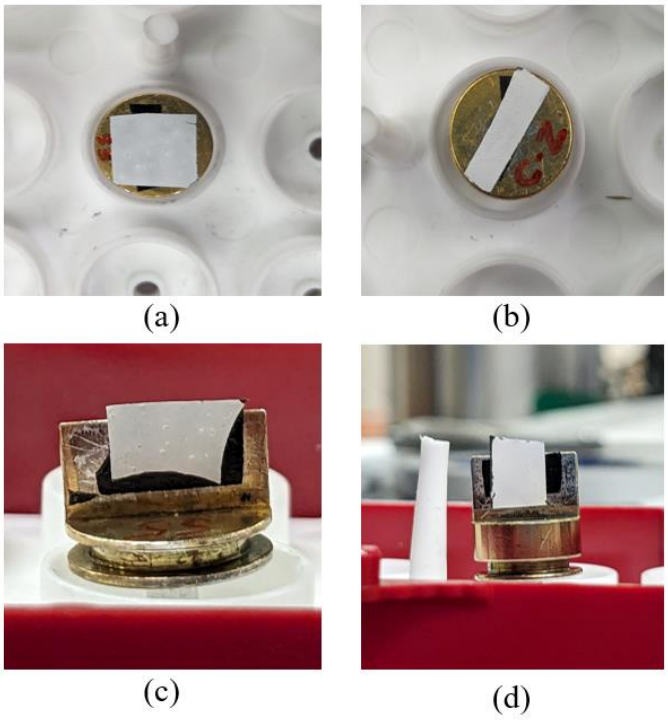


Fig 2.4 Images of (a) lab-scale zeolite and (b) commercial zeolite samples for surface imaging; (c) lab-scale zeolite and (d) commercial zeolite samples for cross-sectional imaging

The samples made are subsequently gold coated to obtain high resolution images. Gold coating enhances the quality of images by preventing the charging of samples and making

them conductive for electrons. Typically, gold coating is done for 90 seconds, resulting in a distinctive brownish color to the samples. The gold coated samples are then viewed under SEM. Figures 2.5(b) and 2.5(c) show the surface and crossectional SEM images of lab-scale zeolite coated onto the NMC, while figures 2.5(e) and 2.5(f) provide a view of surface and crossectional images of commercial zeolite coated onto the NMC, respectively.

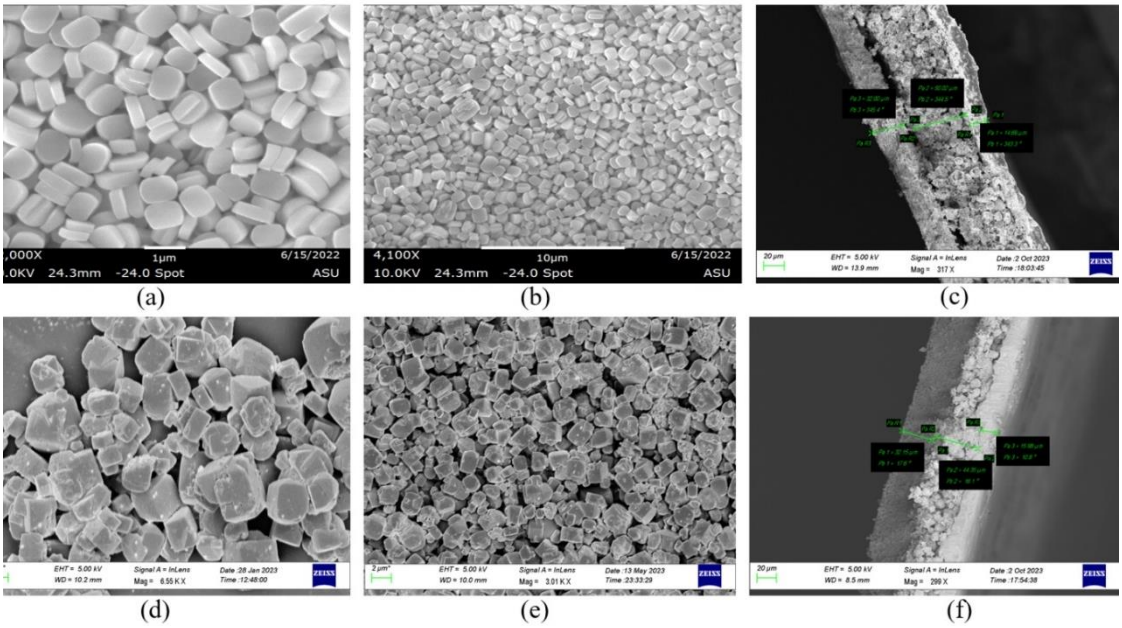


Fig 2.5 SEM images of (a) lab-scale zeolite powder (b) surface of lab-scale zeolite coated on NMC and (c) cross-section of lab-scale zeolite coated on NMC; (d) commercial zeolite powder (e) Surface of commercial zeolite coated on NMC and (f) cross-section of commercial zeolite coated on NMC

From the SEM images of zeolite powders, lab-scale zeolite is more plate structured with a uniform particle size of 2 µm (length) and 400 nm (thickness). The aspect ratio of particles is defined as the ratio of length to the thickness of the particles. Hence, the aspect ratio of

lab-scale zeolite particles is around 5. However, the morphology of commercial zeolite is quite different from lab-scale zeolite. The particles are more spherical in shape with an aspect ratio of 1. Additionally, the particles exhibit non-uniformity with a size range of 1-3 µm. From the images of silicalite and zeolite coated on NMC, it's evident that both coatings have effectively covered the NMC particles as their sizes fall within the same range as the NMC pore size. However, it is important to note that the inter-particle pores in the commercial zeolite separator appear to be more pronounced compared to the lab-scale zeolite coating. Furthermore, from the crossectional images of separators, the thickness of the coatings measured is around 30 µm, which is the final thickness of the separators after shrinkage during drying.

Fourier-Transform Infrared Spectroscopy (FTIR)

To know more about the chemical properties of the commercial zeolite, FTIR technique is utilized. FTIR spectroscopy is an analytical method used to identify various chemical groups such as organic, polymeric, and in certain cases, inorganic materials. This technique uses infrared light to scan the test samples and characterize their chemical properties.

In this method, the infrared radiation is passed through the sample. A part of it is absorbed, and the remaining passes through the sample. The absorbed radiation is converted to rotational and vibrational energy by the molecules of sample, which is detected by the detector in the form of wave number. Every molecule and chemical bond possess a distinct spectral pattern, making FTIR a valuable technique for chemical identification[38]. The FTIR analysis is done for lab-scale zeolite as well to see the similarities in the chemical bonds between the lab made silicate and commercially purchased zeolite.

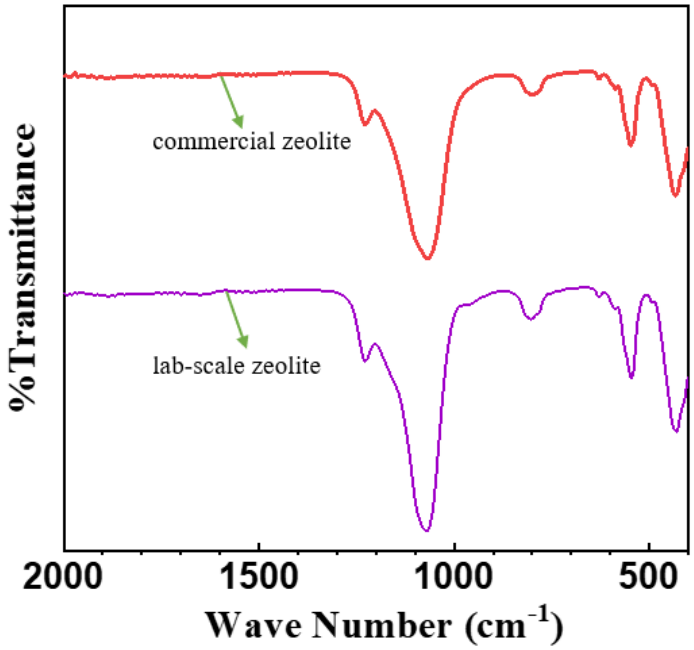


Fig 2.6 FTIR spectrum comparison of Lab-scale zeolite and commercial zeolite

From the above spectrum data, it is evident that the chemical bonds present in the lab made silicalite and commercial zeolite are identical. The table below illustrates the chemical bonds or linkages corresponding to the peaks in the spectrum:

| **Peak wave number ($cm^{-1}$)** | **Chemical Bond/linkage** |
|---|---|
| 430 | Si-O |
| 550 | Si-O-Si |
| 800 | Si-OH |
| 1065 | Si-O-Si |
| 1220 | Si-O |

Table 2.1 Identification of the chemical bonds in zeolites from FTIR spectrum[39][40][41]

The data presented above confirms that, the commercial zeolite is also a pure silica zeolite with no aluminosilicate bonds in it (as there are no more peaks after 2000 till 5000 $cm^{-1}$).

X-ray Diffraction (XRD)

X-ray diffraction (XRD) analysis is done for separators to gain insights into the orientation of particles after they are coated and compressed during the final assembly of coin cells. Initially, the randomly oriented particles are made into a slurry which is coated on to the NMC using a blade coater. Subsequently, they are cut into 16mm circles and utilized for making coin cells. The coin cells are crimped at a pressure of 400 psi. Hence, XRD patterns of the randomly oriented powders, powder coated on NMC, and powder coated NMC compressed at 400 psi are obtained to get better understanding of the crystal orientation throughout the process.

Since the coating of separators is 30 µm thick, the XRD does not detect the underlying cathode. The XRD patterns of commercial zeolite and lab-scale zeolite coated NMC confirms that the zeolites are MFI type zeolites, and the cathode below has been covered uniformly, preventing any possible internal short circuiting. Figures 2.7(a) and (b) show the XRD patterns obtained for powders and separators.

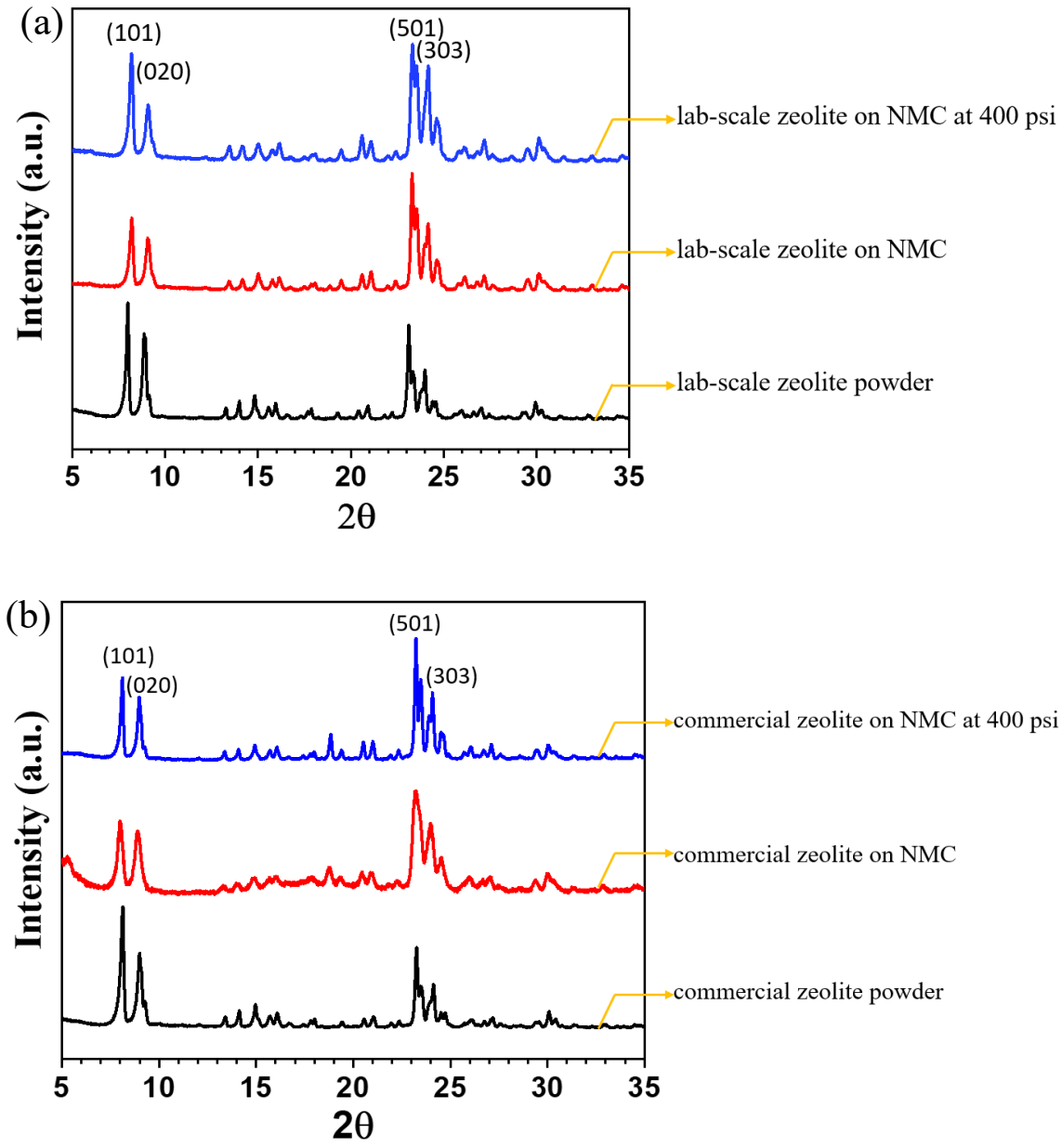


Fig 2.7 XRD patterns of (a) lab-scale zeolite powder, lab-scale zeolite coated on NMC, and lab-scale zeolite coated NMC compressed at 400 psi; (b) commercial zeolite powder, zeolite coated on NMC, and zeolite coated NMC compressed at 400 psi

The SEM images in figure 2.5 show that the lab-scale zeolite crystals lay down flat and are oriented after coating with a blade coater due to their plate shape morphology. On the other

hand, commercial zeolite particles, being more spherical in shape, display random orientation on NMC surface after the blade coating. However, during the fabrication of coin cells, both types of separators are subjected to a compression force of 400 psi.

This compression leads to further alignment of lab-scale zeolite particles and improves the b-orientation of crystals. Nevertheless, the commercial zeolite particles owing to their spherical nature, there is not much improvement seen in the b-orientation plane of the crystals even after compression.

The XRD patterns also reveals the same that after compression, the lab-scale zeolite particles undergo further alignment. However, the reorientation of commercial zeolite particles is not highly pronounced owing to its spherical shape morphology. During the charging and discharging cycles, the transport of the solvated lithium ions is facilitated in the direction of (020) plane between the electrodes.

The surface micrographs in figure 2.8 confirm the XRD results indicating that there is further alignment of lab-scale zeolite particles after compression at 400 psi, but it is not very significant. Post compression, the particles are aligned in such a manner where the micropores are oriented perpendicular to the surface area, making the pores face towards the electrodes whereas in the instance of commercial zeolite, even with compression, there is minimal enhancement observed in the orientation of crystals.

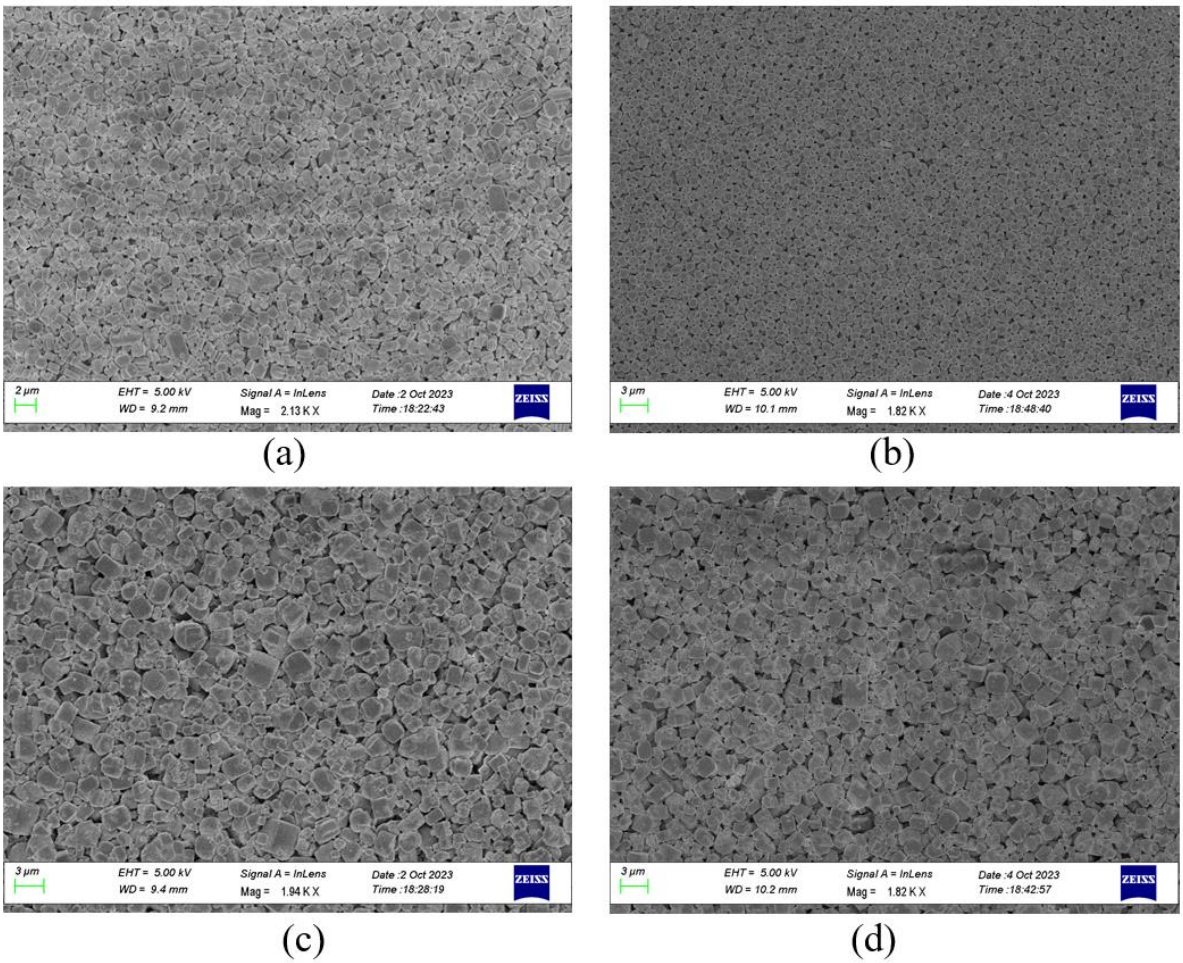


Fig 2.8 SEM images of lab-scale zeolite coated NMC (a) before and (b) after compression; commercial zeolite coated NMC (a) before and (b) after compression

Contact Angle

To assess the wettability of lab-scale zeolite and commercial zeolite separators, a single sessile drop wettability test is performed on both the separators. To measure the contact angle, 1M $LiPF_6$ in 1:1:1 (v/v/v) ethylcarbonate/dimethylcarbonate/diethylcarbonate electrolyte is used. A drop of the electrolyte is dispensed against the separators and contact angle is measured.

To make the separators for contact angle measurement, initially, a slurry is prepared by mixing these powders with 5 wt% polyvinyl alcohol aqueous solution, which acts as a binder, and water, which serves as a solvent. The Composition of the slurries is mentioned in the table below:

| | **Mass of Powder** | **Mass of 5 wt% PVA aqueous solution** | **Mass of Water** |
|---|---|---|---|
| Lab-scale zeolite | 1 gm | 1 gm | 0.5gm |
| Commercial zeolite | 2.5 gm | 0.5 gm | 2 gm |

Table 2.2 Composition of the components in the slurry

Once the slurries are made, they are coated onto the NCM cathode with a thickness of 40 micrometers using a doctor blade. Then the separators are dried in a humid chamber at 40℃ and 60% relative humidity for 8 hours. This is followed by an additional step of drying in vacuum oven at 70 ℃ for 12 hours. Once the drying process is completed, the separator samples are prepared for contact angle measurement. The equipment used to measure the contact angle is Kruss Easy drop goniometer. The results of the measurement are as follows:

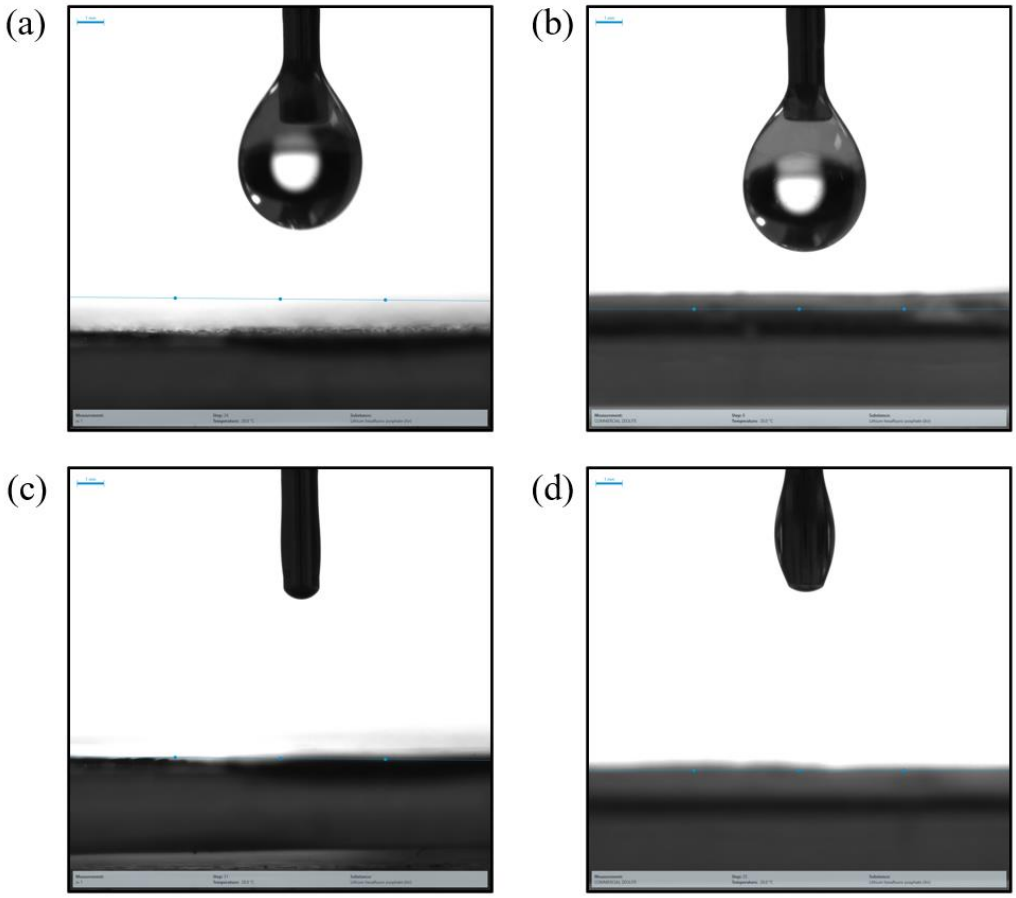


Fig 2.9 At t = 0 sec, the electrolyte drop against (a) lab-scale zeolite and (b) commercial zeolite separators; at t = 1 sec, the electrolyte drop on (a) lab-scale zeolite and (d) commercial zeolite separators

The contact angle of both the separators is zero. As soon as the electrolyte is dropped onto the separators, the drop is elapsed, and the contact angle measured is zero. From the above results it can be inferred that the lab-scale zeolite and commercial zeolite separators are highly wettable and have better electrolyte uptake. This explains the microporous nature of zeolites and high surface energy of the inorganic separators.

Thermo-Gravimetry and Differential Scanning Calorimetry (TGA/DSC)

To examine the thermal stability and heat flux characteristics of the separators, TGA/DSC techniques are used. TGA explains weight loss while the DSC measures the changes in the physical properties with temperature and time.

To perform this characterization technique, free-standing lab-scale zeolite and commercial zeolite separators are made. Initially, slurry of the powders are made to coat them on Al foil. 1 gram of 5 wt% PVA aqueous solution and 0.5 gram of water are added to 1 gram of lab-scale zeolite powder and 0.5 grams of 5 wt% PVA aqueous solution, 2 grams of water are added to 2.5 grams of commercial zeolite powder to make their slurries.

The slurries are now coated onto an aluminum foil of 7inch*7inch, using a blade coater to about 50 micrometers thickness. The coatings are dried in a humid chamber at 40 ℃ and 60% relative humidity for 8 hours. Subsequently, they are dried in a vacuum oven at 70 ℃ for 12 hours. Now, the coated separators are peeled off carefully from the aluminum foil to make free-standing separators. The peeled separators are broken into small pieces to fit them into the crucible and tested for TGA/DSC (Labsys Evo from Setaram). The samples are heated from 20 ℃ to 400 ℃ at a rate of 10 ℃/min in the atmosphere of ultra-pure air. The results look like:

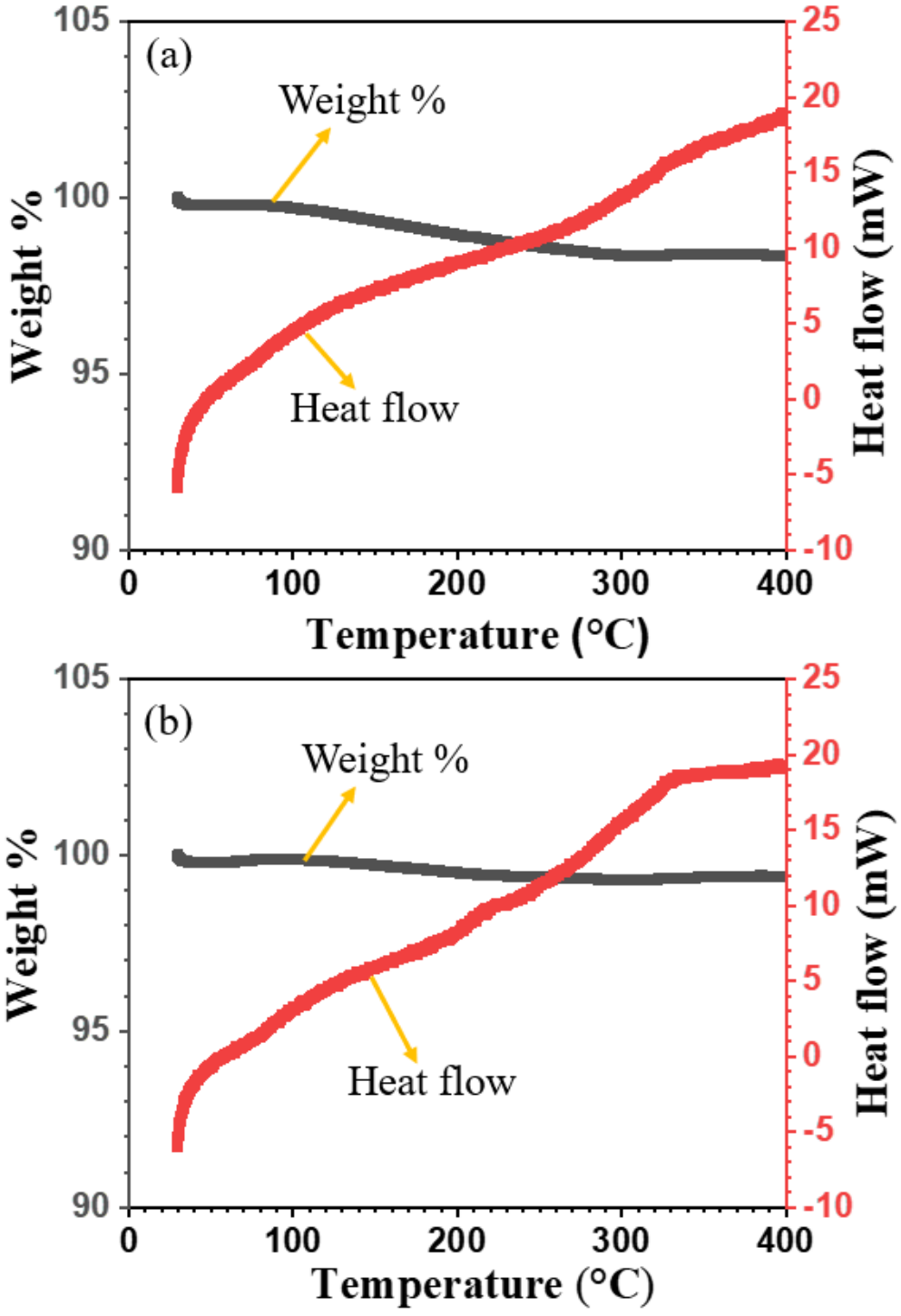


Fig 2.10 TGA/DSC curves of (a) lab-scale zeolite (b) commercial zeolite separator

From the results of TGA, there is approximately 2% and 0.5% of mass loss observed with lab-scale zeolite and commercial zeolite separators, respectively. The mass loss incurred is not very significant. However, this loss can be attributed to the release of entrapped gases and water vapor absorbed by the zeolites. Furthermore, there are no discernible peaks in the DSC analysis indicating the separators are thermally stable. Though the separator contain PVA, the total amount of it is significantly low compared to the zeolite and water content. Thus, it has a very negligible effect on the thermal performance of the separator.

### 2.3.2 Electrochemical Performance of Zeolite Separators

In this study, full cells are made using NMC as cathode and graphite as anode with lab-scale zeolite and commercial zeolite coated on NMC as separators and 1M $LiPF_6$ in EC/DEC/DMC (1:1:1 v/v/v) as electrolyte. The constructed cells are tested for their charge-discharge characteristics, capacity density and electrochemical impedance.

The cells are cycled using CC-CV method and Fig 2.11(a) shows the $1^{st}$ and $50^{th}$ cycle for lab-scale zeolite, while Fig 2.11(b) shows for commercial zeolite cycled at 0.1 C rate. The theoretical capacity of cathode used in this study is 155 mAh/g with a mass loading of 121 $g/m^2$. The capacity density given by the full cells of lab-scale zeolite, and commercial zeolite separators is about 160 and 153 mAh/g, respectively. The charge and discharge curves for both the separators look same as both of them are microporous in nature. However, when comparing the lab-scale zeolite separator to the commercial zeolite separator, it becomes evident that the former exhibits higher capacity density. This difference can be attributed to the morphological differences between these zeolites, particularly in terms of particle shape and size.

The better capacity density of lab-scale zeolite is due to the uniform diffusion of solvated Li-ions through the intraparticle pores within zeolite resulting in the formation of more uniform and stable SEI. This uniform Li-ion flux through intraparticle pores is facilitated by good b-orientation of crystals in lab-scale zeolite.

Li-ion flux solely through the inter-particle pores is usually not very uniform resulting in the formation of unstable and non-uniform SEI that break down on continuous cycling and resulting in fading of capacity. However, the intra-particle pores of zeolites help with homogenizing the Li-ion flux at separator-anode interface resulting in the formation of stable and uniform SEI layer which leads to long cycle life of coin cells due to the minimal losses of active lithium-ions. Therefore, despite the lower capacity density of the commercial zeolite in comparison to lab-scale zeolite, it still exhibits good capacity retention and stability.

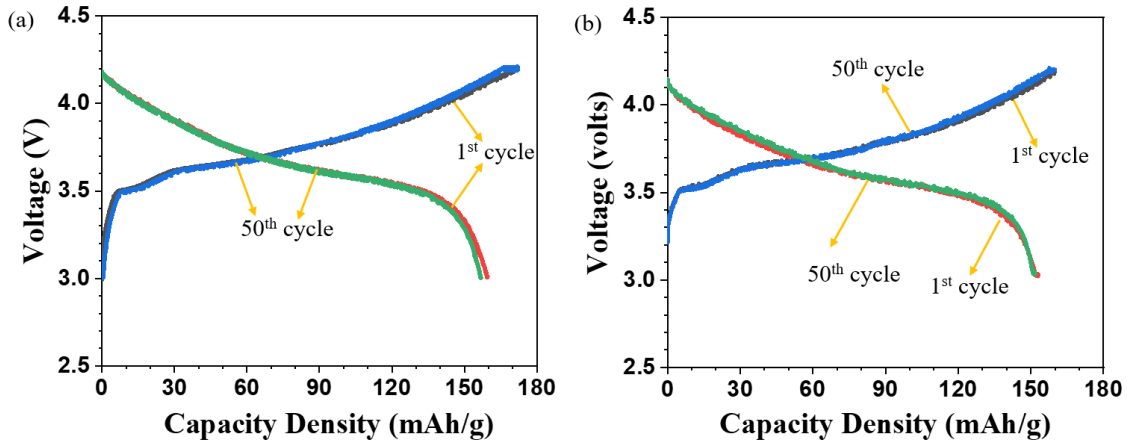


Fig 2.11 CC-CV curves for charge and discharge cycles of (a) Lab-scale zeolite and (b) Commercial zeolite separator cells at 0.1 C rate

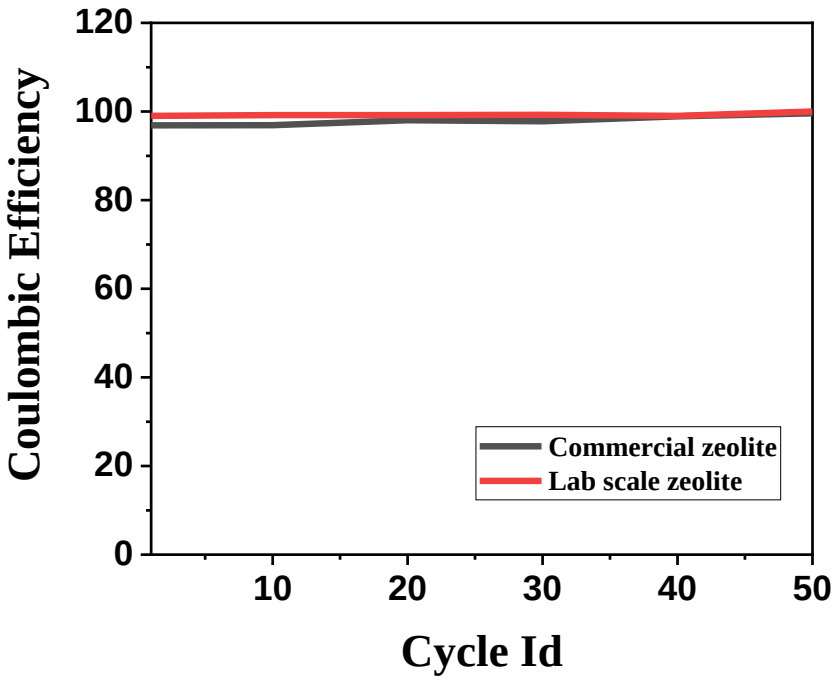


Fig 2.12 Coulombic Efficiency of zeolite separators

Electrochemical Impedance Spectroscopy (EIS)

The same cell configurations are tested for electrochemical impedance spectrometer (EIS) and Nyquist plots are generated for the full cells. These plots are obtained by applying a frequency range of 100 KHz to 1.5 Hz with an AC amplitude of 10 mV rms. Subsequently, the plots are analyzed in EC lab software to get the impedance parameters. The circuit is composed of three types of resistance, 1. Ohmic resistance, 2. Resistance due to SEI and 3. Resistance due to charge transfer. Fig 2.12 shows the Nyquist plots of lab-scale zeolite and commercial zeolite separator full cells from the EIS, and Table 2.3 gives the impedance parameters of each cell.

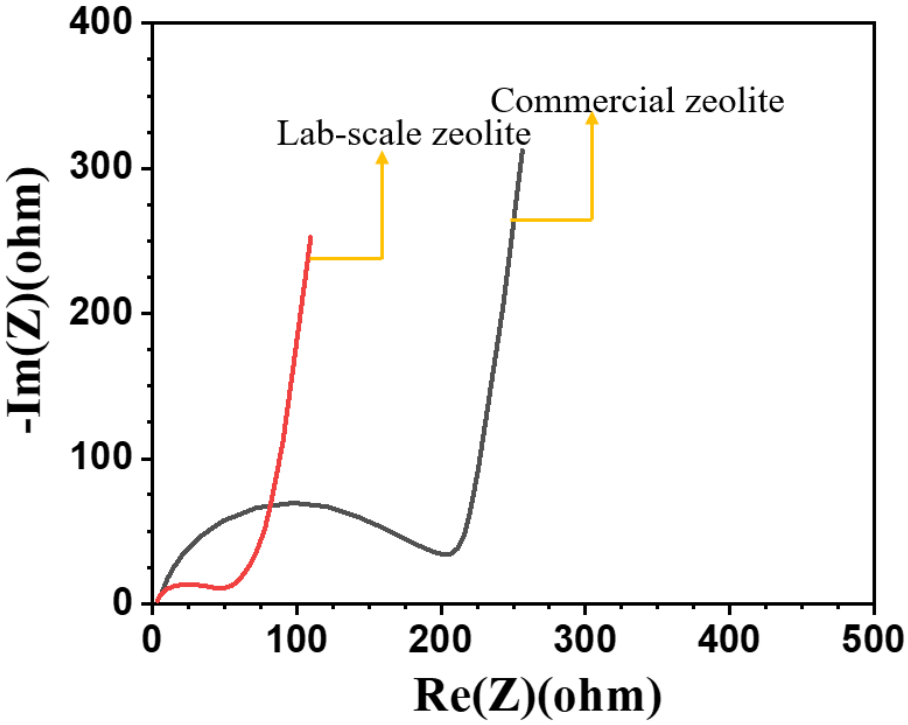


Fig 2.13 Nyquist plots of commercial zeolite and lab-scale zeolite separator full cells

| Zeolite | Thickness | $R_{ohmic}$ | $R_{SEI}$ | $R_{charge\ transfer}$ |
|---|---|---|---|---|
| Commercial Zeolite | 40 | 3.74 | 205 | 200 |
| Lab-scale zeolite | 40 | 3.8 | 65 | 190 |

Table 2.3 Impedance parameters of lab-scale zeolite and commercial zeolite full cells

The Nyquist plots above are analyzed in EC lab to obtain impedance parameters which are reported in table 2.3. The ohmic resistance is due to the electrolyte within the separator. The low value of the ohmic resistance of commercial zeolite separator compared to lab-

scale zeolite suggests that it have better electrolyte uptake, which can be attributed to its high wettability and inter-particle porosity that can be calculated from equation 2.1. However, the SEI and charge transfer resistance of lab-scale zeolite is significantly lower than that of commercial zeolite indicating the formation of uniform SEI at the anode surface due to the uniform Li-ion flux through the intraparticle pores of the separator.

## 2.4 Summary

The charge and discharge curves of lab-scale zeolite and commercial zeolite separators are similar due to the microporous nature of the zeolites. However, lab-scale zeolite shows more capacity density compared to commercial zeolite. This is due to the difference in the particle morphology. But the commercial zeolite separator have also demonstrated excellent capacity retention and stability due to the presence of intraparticle pores. Furthermore, the ohmic resistance of commercial zeolite separator is notably low indicating that the separator have good electrolyte uptake and wettability because of its high porosity. However, the SEI resistance of lab-scale zeolite is significantly lower than that of commercial zeolite suggesting the formation of uniform and stable SEI due to the uniform Li-ion flux at the anode, facilitated by the crystal orientation. This uniform SEI contributes to its high capacity which is consistent with the performance observed in the CC-CV cycles. Therefore, due to the challenges encountered in scaling up of the synthesis of lab-scale zeolite, this commercial zeolite procured can be considered as a viable option for upscaling electrode-coated separators.

# CHAPTER 3

# OPTIMIZATION OF PARTICLE SIZE OF SILICALITE FOR IMPROVED PERFORMANCE OF Li-ION AND Li-METAL BATTERIES

## 3.1 Introduction

Currently, Lithium-ion batteries stand as the most effective energy storage solution. However, lithium-metal batteries are emerging as the potential successors to the Li-ion battery system due to their high theoretical specific capacity. In lithium metal batteries, the anode is lithium metal. Lithium, being a highly reactive metal, reacts with the conventional organic electrolytes resulting in the formation of solid-electrolyte interface (SEI). But the SEI formed is not very stable and lacks mechanical robustness. It tends to break down on continuous cycling, exposing the bare lithium to the electrolyte. As a result, continuous loss of capacity of the battery could be seen[42].

Additionally, the points where SEI breaks serve as localized high concentration zones for the migration of lithium ions and results in the formation of Lithium dendrites. With further cycling, non-uniform lithium plating could be observed. At high current densities, the dendrites propagate from anode to cathode piercing through the separator causing an internal-short circuit. This could potentially lead to thermal runaway and cause fire hazard or explosion[42][43].

Recently, Kishen and et al. published a paper on zeolite separators for fast charging and dendrite-free lithium metal batteries[43] in which it is inferred that plate silicalite separator coated on NMC exhibits excellent safety and electrochemical performance compared to the similar tortuously porous gama alumina separators. Plate silicalite, being tortuous with

intraparticle pores, enables fast charging and dendrite-free lithium-ion/lithium-metal batteries. The intraparticle pores within the zeolite separator particles provide a more effective means of homogenizing the Li-ion flux at the interface between the separator and the anode that enables the stable operation of lithium-metal batteries even at high C-rates compared to the gama alumina separator with same tortuosity. The Li-ion flux in gama alumina separator is only through the interparticle pores due to which a non-uniform SEI is formed on the anode, and loss of capacity is observed on continuous cycling. High tortuosity of both the separator signifies a longer path for transversal, resulting in greater resistance to the dendrite propagation. Thus, the intraparticle pores and high tortuosity of plate silicalite separators significantly contributes to the development of dendrite free high performance lithium-metal batteries.

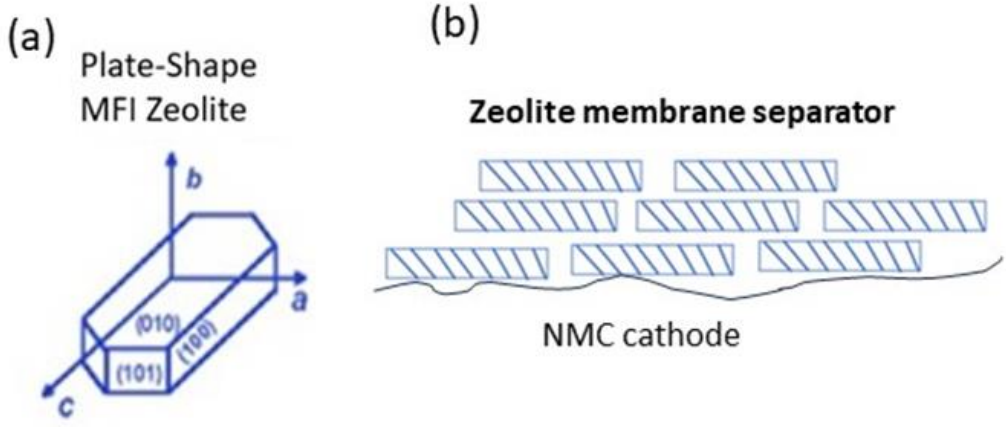


Fig 3.1 Schematic illustration of (a) plate-shaped MFI zeolite crystal showing crystallographic planes and (b) structure of membrane separator made of plate-shaped zeolite on NMC cathode after compression[43]

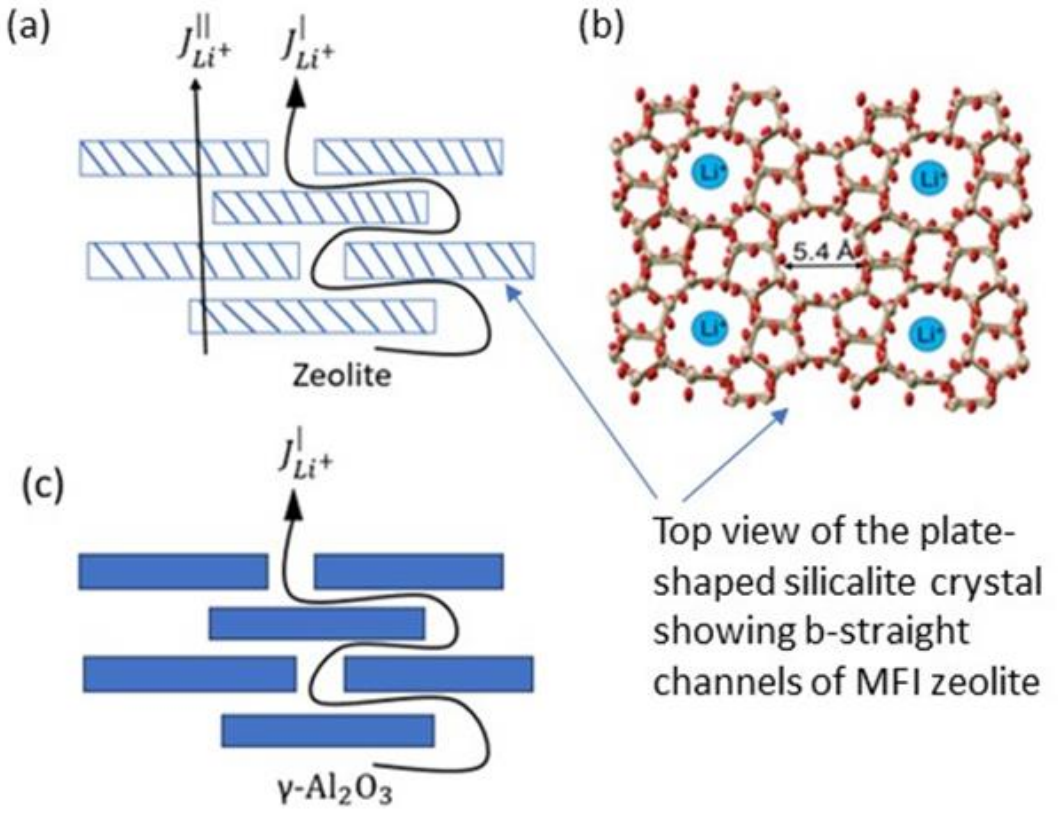


Fig 3.2 (a) Schematic illustration of two pathways for lithium-ion flux through electrolyte-filled separator made of plate-shaped MFI zeolite with (b) top view of b-axis crystalline pore structure of MFI zeolite and (c) schematic illustration of one pathway for lithium-ion flux through electrolyte-filled separator made of dense plate-shaped γ-alumina particles[43]

To commercialize the plate silicalite coated separators, it is essential to scale-up the synthesis of plate silicalite to obtain the required quantity of powder for coating. However, as mentioned in the research objective the laboratory synthesis method used to make the silicalite presents significant challenges for effective upscaling. In the current synthesis

process, plate silicalite is generated without any agitation of the solution during the crystallization phase, resulting in a low yield and non-uniform particle size.

This chapter of thesis primarily focus on modifying the process conditions of the existing synthesis method to achieve (a) uniform size particles with improved yield for effective scaling up of silicalite synthesis and (b) large aspect ratio particles for developing highly tortuous separator to inhibit dendrite propagation for safe Li-ion batteries.

## 3.2 Experimentation

### Synthesis of plate silicalite

The procedure for making plate silicalite in laboratory reported by Kishan and et al. is as follows[43]:

First 4 grams of TPAOH is added to 170 grams of DI water followed by the addition of 10 grams of TEOS while stirring the solution. The beaker is sealed with a paraffin wax film and stirred for 24 hours at room temperature to obtain a clear solution. Subsequently, the solution is divided into two 100ml autoclaves and the autoclaves are placed in the oven which is preheated to 155 ℃. The solution filled autoclaves are heated for 10 hours at that temperature in stagnant condition. After the completion of the hydrothermal synthesis, mother liquor is drained and silicalite particles are recovered. Then the crystals are washed with DI water and centrifuged at 10,000 rpm for 20 mins. The washing and centrifugation are repeated for at least three times, and the crystals are dried at 120 ℃ in a vacuum chamber to remove any traces of water present. The final step is calcination where the powder is heated at 600 ℃ for 18hrs in a furnace for the removal of organic template.

While modifying the above process conditions, the initial step involves altering the molar ratios of the precursors within the seeding solution. The ratios are carefully chosen to yield particles of size 2-3 μm. This specific size of particles is imperative to ensure effective coating on the NMC, as the pore size of NMC cathode falls within the same range. Therefore, an extensive exploration of literature is done to identify a molar ratio that can produce the desired particle size with coffin shape. A previous study by Fateme et al. on template free synthesis of Highly B-oriented MFI type zeolite thin films by seeded secondary growth [44], reported the synthesis of plate silicalite with a particle size of 2 μm. Thus, the molar ratios of the precursors in the modified synthesis is adopted from this particular work. The altered molar ratios looks like: TEOS:0.15TPAOH:103.5$H_2O$.

**The procedure to synthesize plate silicalite under modified conditions goes like:**

The calculated quantities of TEOS, TPAOH, and DI water from the above chosen molar ratios are 4.166 g, 3.036 g, and 34.833 g, respectively. Initially, the calculated amount of TPAOH is added to water, and the solution is stirred at 350 rpm for ten mins. Subsequently, the required amount of TEOS is added to the stirring solution, and the stirring speed is increased to either 500 or 550 rpm. The stirring is done at room temperature for 24 hrs. After 24 hrs of stirring, the solution is left undisturbed and aged for an additional time of 48 hrs.

Following the aging period, the solution is transferred into a 50ml autoclave. For stirring purposes, a rotary mixing ball mill from MTI Corporation is utilized. This equipment includes two 50 ml autoclave holders that rotate in circular motion. During rotation, both autoclaves should have the same weight. Therefore, while making seeding solution, two

beakers of solution are made. The aged solution is then taken into the two autoclaves, and different combinations of temperatures and times are applied.

The temperatures and times used are 140 ℃, 155 ℃, 175 ℃, and 8 hrs, 10 hrs, 12hrs, 15hrs, respectively. For all the combinations, the stirring speed used is 40 rpm. After the hydrothermal process, crystals are recovered and washed with DI water. Later, the solution is centrifuged at 10,000 rpm for 20 mins. This process of washing and centrifugation is carried out three times, followed by the drying of powder at 100 ℃ for 24 hrs. Then, the powder obtained is calcined at 650 ℃ for 18 hours. Finally, the powders are viewed under SEM to examine their morphology and particle size

### 3.3 Results and Discussion

#### 3.3.1 Plate silicalite synthesized under stagnant conditions

Yield of the process

The yield of the synthesis is calculated as follows:

Amount of TEOS = 10 grams = 10.718ml ($\rho$ = 0.933 g/ml at 25 ℃)

Amount of TPAOH = 4 grams = 3.952 ml ($\rho$ = 1.012 g/ml at 25 ℃)

Amount of DI water = 170 grams = 170 ml

Total volume of solution = 184.67 ml

The amount of powder obtained from 100 ml of solution is 0.6 grams

Amount of TEOS in 100 ml of seeding solution = $\frac{100}{184.67} \times 10 = 5.415$ g = 0.026 mol

$\therefore$ Amount of silica $= 0.026 \times 60 = 1.56$ grams

The actual amount of silica obtained from the process $= 0.6$ grams

$\therefore$ Yield $= \frac{0.6}{1.56} \times 100 = 38.416\%$

The plate silicalite produced using the method guided by Kishen et al. is observed under scanning electron microscope to know more about the particle size and shape. The figures below are the SEM images of the plate silicalite:

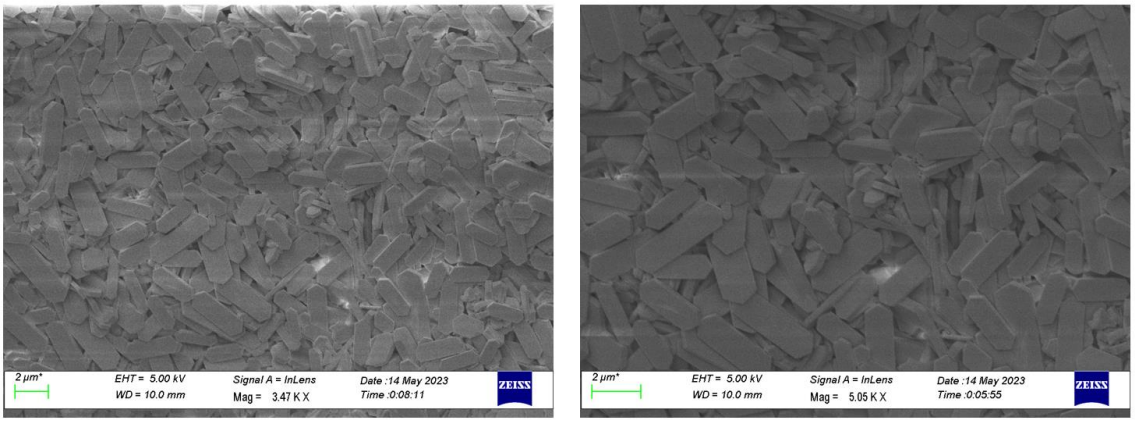


Fig 3.3 SEM images of plate silicalite powder produced under stagnant conditions

The SEM image reveals that the particles length varies between 2 to 8 µm and the thickness is in the range of 0.1 to 0.2 µm. These values of length and thickness give an aspect ratio of around 40, indicating that the particles are predominantly two-dimensional (2-d).

Typically, on an industrial scale, zeolites are synthesized with continuous stirring. The non-uniform size of particles and low yield of the above process could be the consequence of the production of silicalite under stagnant conditions during the hydrothermal synthesis. The crystallization occurring does not have any form of agitation. Autoclaves are simply positioned inside the oven where the solution remains stagnant without any stirring mechanism. In the process of hydrothermal synthesis, incorporation of solution stirring enhance consistent crystallization resulting in more uniform size particles and improved

overall yield of the process. Additionally, the stirring can help in effective scaling up of the process.

### 3.3.2 Plate silicalite synthesized under stirring conditions

The plate silicalites obtained from modified process conditions are viewed under SEM to gain insights into the morphology of particles. Obtaining clear SEM images for powder samples can be challenging, as charging of particles can occur and decrease the resolution of the image. Hence, a slightly different approach is employed for the preparation of these powder samples.

Sample preparation for SEM imaging

The detailed procedure is:

1. Take a 7ml glass vial and fill more than half of the volume with methanol (methanol is used to disperse the zeolite rather than dissolving it).
2. Add a small amount of powder to the methanol in the vial.
3. The mixture is sonicated for 2 hours to break any aggregate of particles present.
4. Cut a microscopic slide into small pieces and mount a piece onto the sample holder with the help of carbon tape.
5. Using a micropipette, a drop of sonicated mixture is put on the mounted glass slide.
6. The sample is allowed to dry in a minimum particle contamination environment.
7. Now, gold coat the sample for 180 sec before viewing it under the SEM.

Figures 3.4, 3.5 and 3.6 show the SEM images of plate silicalite particles synthesized at different temperatures and times under stirring conditions.

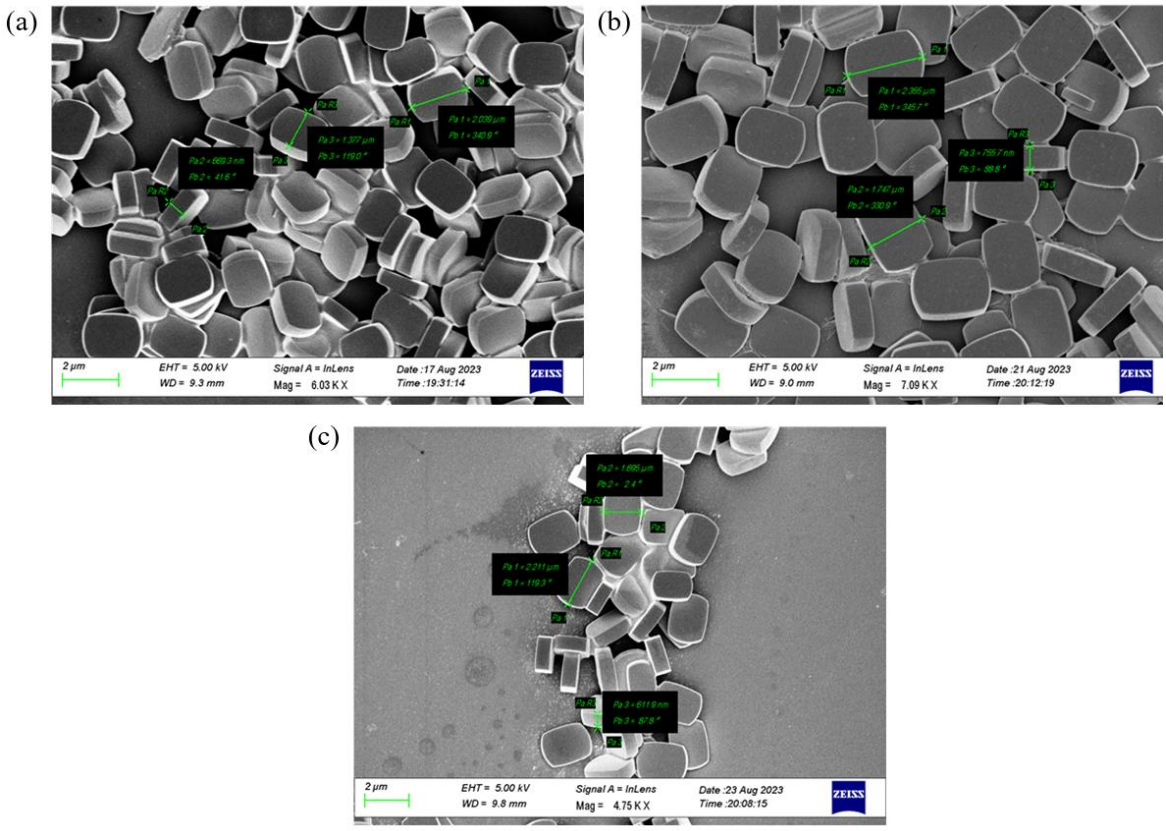


Fig 3.4 SEM micrographs of plate silicalite particles made at (a) 140 ℃, 8 hrs, 40 rpm (b) 140 ℃, 10 hrs, 40 rpm (c) 140 ℃, 12 hrs, 40 rpm

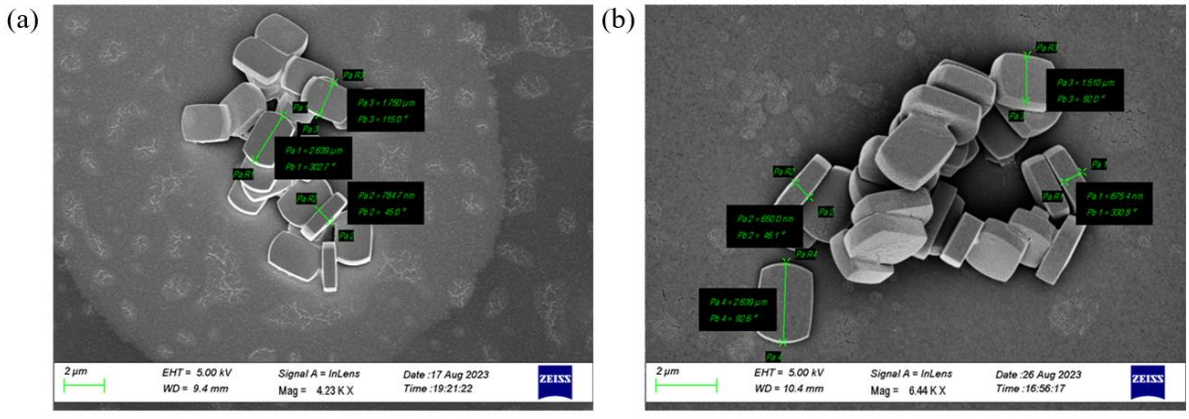


Fig 3.5 SEM images of plate silicalite made at (a) 155 ℃, 10 hrs, 40 rpm and (b) 155 ℃, 12 hrs, 40 rpm

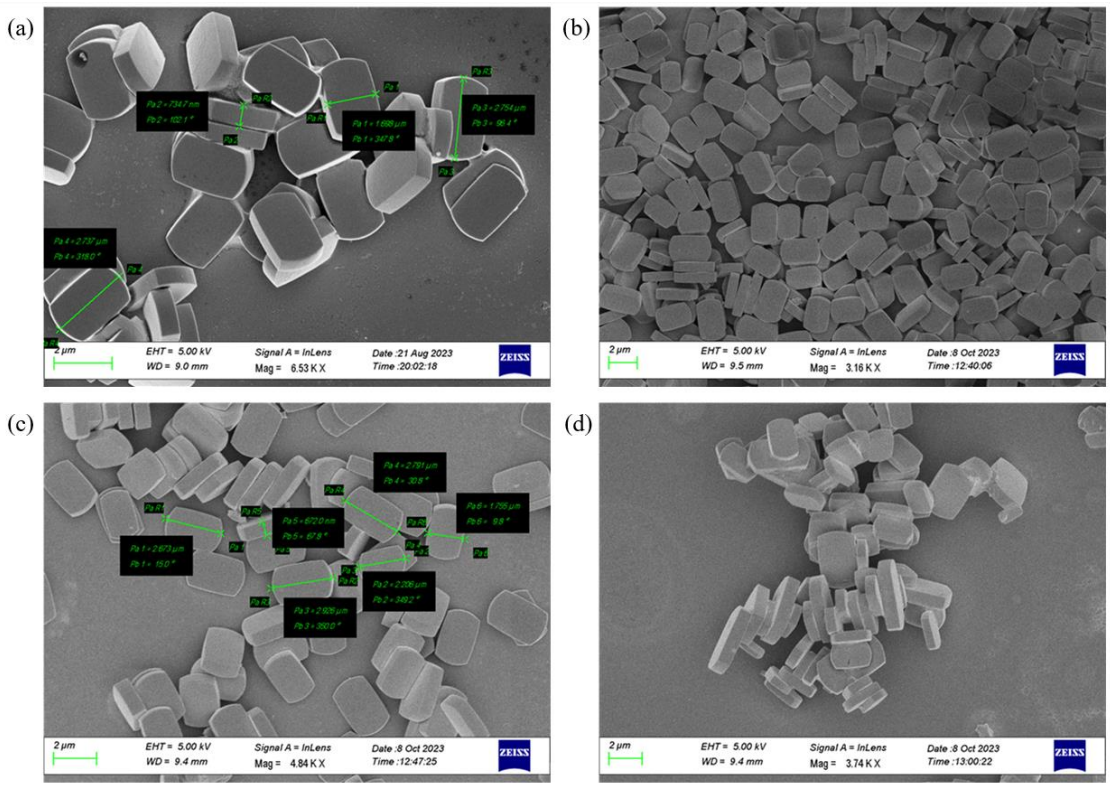


Fig 3.6 SEM images of plate silicalite made at (a) 175 ℃, 8 hrs, 40 rpm, (b) 175 ℃, 10 hrs, 40 rpm, (c) 175 ℃, 12 hrs, 40 rpm and (d) 175 ℃, 15 hrs, 40 rpm

The details of all the batches of powder obtained are reported in the table below:

| Property/Zeolite | 140 ℃, 8 hrs | 140 ℃, 10 hrs | 140 ℃, 12 hrs | 155 ℃, 10 hrs | 155 ℃, 12 hrs | 175 ℃, 8 hrs | 175 ℃, 10 hrs | 175 ℃, 12 hrs | 175 ℃, 15 hrs |
|---|---|---|---|---|---|---|---|---|---|
| Length (µm) | 2.039 | 2.35 | 2.211 | 2.64 | 2.639 | 2.78 | 2.848 | 2.6-2.8 | 2.475-3.035 |
| Breadth (µm) | 1.37 | 1.74 | 1.695 | 1.75 | 1.51 | 1.69 | 1.789 | 1.742 | 1.761 |
| Width (µm) | 0.67 | 0.755 | 0.611 | 0.784 | 0.650 | 0.734 | 0.654 | 0.647 | 0.654 |
| Aspect ratio | 3.04 | 3.11 | 3.61 | 3.36 | 4.06 | 3.78 | 4.35 | 4.01-4.32 | 3.78-4.64 |
| Amount of powder obtained (g) | 1.1 | 1.1065 | 1.1365 | 1.135 | 1.114 | 1.134 | 1.385 | 1.1285 | 1.1195 |
| Theoretical mass (g) | 1.1998 | 1.1998 | 1.1998 | 1.1998 | 1.1998 | 1.1998 | 1.1998 | 1.1998 | 1.1998 |
| Yield % | 91 | 92 | 94.724 | 94 | 92.89 | 94.55 | 94.89 | 94.057 | 93.30 |

Table 3.1 Properties of different batches of plate silicalite powders

From the SEM images, dimensions and aspect ratio of particles obtained at different temperatures and times are reported in Table 3.1. It provides clear insights into how increasing temperature and time of crystallization under stirring conditions resulted in larger particle sizes and improved process yield. However, there is no significant change observed in the aspect ratio of the particles due to the increase in thickness of the crystals. To have a higher aspect ratio, it is essential for the particles to exhibit 2-dimensional structure with minimum thickness. Moreover, it is observed that at elevated temperatures, particles tend to exhibit non-uniformity in size and have a size distribution.

Hence, with the molar composition we chose , by varying temperatures from 140 to 175 ℃ and times from 8 to 15 hrs, there is not much change observed in the aspect ratio. Thus, achieving higher aspect ratios may necessitate a closer examination and potential manipulation of the molar compositions of precursors in the solution.

The X-ray diffraction peaks of two plate silicalite powder samples (140 ℃, 10 hrs, 40 rpm; 155 ℃, 10 hrs, 40 rpm) are measured to see what kind of peaks will be obtained. The results are:

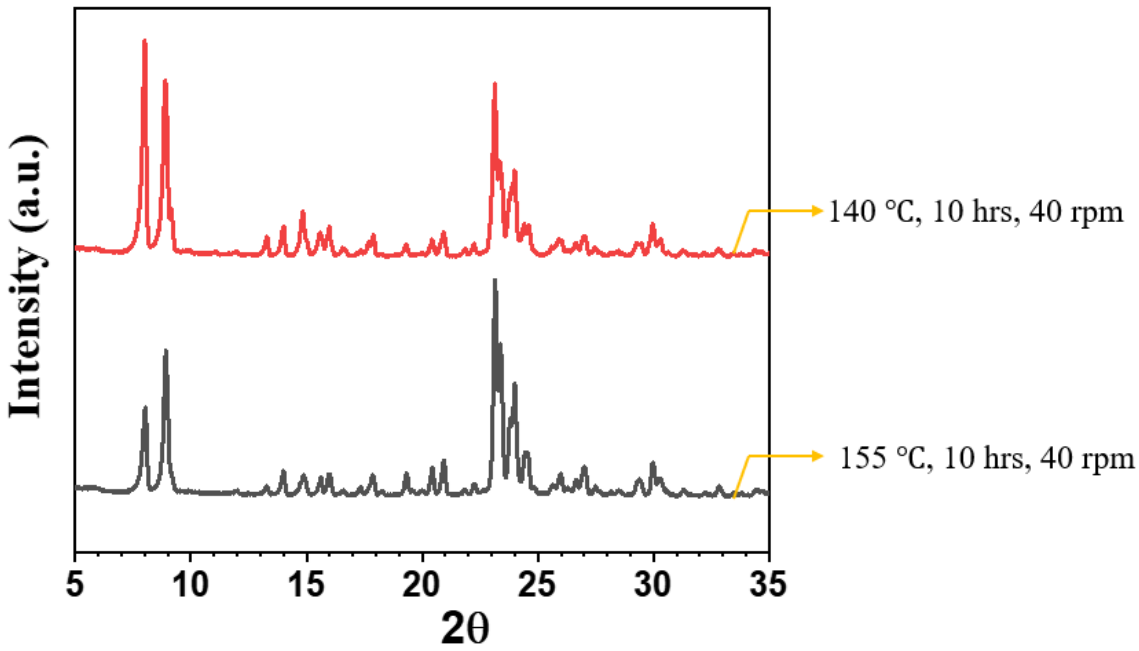


Fig 3.7 X-ray diffraction peaks of two powder samples (140 ℃, 10 hrs, 40 rpm, 155 ℃, 10 hrs, 40 rpm)

The above diffraction peaks confirm the SEM results. From both the characterization techniques, it is evident that plate silicalite obtained by modifying the process conditions is MFI type zeolite. The intensity of the b-orientation (020) peak can be enhanced when the powder is coated onto the NMC and compressed at 400 psi. After compression, all the particles maintain a flat orientation on the surface of NMC, aligning perpendicularly to the direction of Li-ion flux.

**3.4 Summary**

To effectively suppress the propagation of lithium dendrites in lithium-metal batteries, a separator with high durability, tortuosity, and mechanical stability is essential. The Plate silicalite separator demonstrated exceptional performance in addressing lithium-ion

dendrites and enables fast charging of lithium-metal batteries. However, the lab-made plate silicalite encounters multiple challenges when it comes to scaling up due to the absence of stirring in the crystallization phase.

The synthesis under stagnant conditions give non-uniform size particles along with a poor yield of the process. As a result, the synthesis procedure is modified and agitation is introduced during the hydrothermal synthesis with an aim to enhance the uniformity of particles, yield of process and gain more control over particle size.

Stirring of solution during the crystallization phase have improved the uniformity of particles and process yield. Additionally, the increase in temperature and time during hydrothermal synthesis resulted in larger particle sizes. However, it does not significantly alter the aspect ratio of particles. Therefore, further research is necessary to enhance the aspect ratios. This entails achieving a situation where the crystals have the same length as achieved while reducing their thickness to a few nanometers.

# CHAPTER 4

# CONCLUSIONS AND RECOMMENDATIONS

## 4.1 Conclusions

- The process of making slurry and coating it onto the NMC as a separator is initially designed for the lab-scale zeolite. The procedure is successfully reproduced to make a commercial zeolite separator.
- The coated separators exhibited excellent electrolyte wettability, thermal stability, and effective particle packing.
- Lab-scale zeolite and commercial zeolite separators are used to construct coin cells with 1.0M $LiPF_6$ in 1:1:1 (v/v/v) EC/DEC/DMC and have been tested for their electrochemical performance.
- Lab-scale zeolite separator have shown better capacity density compared to commercial zeolite separator and it is due to the difference in morphology such as particle shape of both the zeolites. However, the commercial zeolite separator have also exhibited promising capacity density with excellent capacity retention, stability. It also displayed good performance in terms of charge and discharge cycles.
- Thus, the commercial zeolite procured can be effectively used for the scaling up of electrode-coated separators for developing safe lithium-ion batteries.
- The scalability of the silicalite production became challenging due to the absence of agitation during crystallization.

- By incorporating stirring during crystallization, notable improvements in both process yield, and particle size uniformity are seen.
- Also, the increase in time and temperature during the crystallization phase improved particle size and thickness, leaving no significant change in the aspect ratio of particles.
- It is important to achieve high aspect ratio of particles for creating a highly tortuous separator capable of resisting the propagation of lithium dendrites.
- Therefore, further investigation has to be done on altering the composition of precursors in the seeding solution to improve the aspect ratio. Additionally, the use of various modifiers to achieve the desired morphology and aspect ratio can also be explored.

**4.2 Recommendations**

Based on the findings presented in this thesis, there are specific future recommendations that could potentially advance our research and give a better understanding:

1. Evaluating the electrochemical performance of commercial zeolite and lab-scale zeolite separators at higher C-rates, such as 0.5, 1, and 2 C rates, to gain insights into their potential under different operating C rate conditions.
2. Investigate the performance of the commercial zeolite with 5.3M LIFSI in TMP electrolyte and compare it to the performance with 1.0M $LiPF_6$ in 1:1:1 (v/v/v) EC/DEC/DMC.
3. Further research on controlling particle size and aspect ratio by modifying the synthesis conditions is needed. The study should aim at developing an efficient

scaling-up process capable of producing plate silicalite on an industrial scale, ensuring uniform particle size in the range of 2-2.5 μm with an aspect ratio of 40 while maintaining a high yield.

REFERENCES

[1] Geldasa, F. T., Kebede, M. A., Shura, M. W., & Hone, F. G. (2022). Identifying surface degradation, mechanical failure, and thermal instability phenomena of high energy density Ni-rich NCM cathode materials for lithiumion batteries: A review. In *RSC Advances* (Vol. 12, Issue 10, pp. 5891–5909). Royal Society of Chemistry. https://doi.org/10.1039/d1ra08401a

[2] Wang, Q., Ping, P., Zhao, X., Chu, G., Sun, J., & Chen, C. (2012). Thermal runaway caused fire and explosion of lithium ion battery. In *Journal of Power Sources* (Vol. 208, pp. 210–224). Elsevier B.V. https://doi.org/10.1016/j.jpowsour.2012.02.038

[3] Klein, S., Bärmann, P., Beuse, T., Borzutzki, K., Frerichs, J. E., Kasnatscheew, J., Winter, M., & Placke, T. (2021). Exploiting the Degradation Mechanism of NCM523‖ Graphite Lithium-Ion Full Cells Operated at High Voltage. *ChemSusChem*, *14*(2), 595–613. https://doi.org/10.1002/cssc.202002113

[4] van Schalkwijk Walter and Scrosati, B. (2002). Advances in Lithium Ion Batteries Introduction. In B. van Schalkwijk Walter A. and Scrosati (Ed.), *Advances in Lithium-Ion Batteries* (pp. 1–5). Springer US. https://doi.org/10.1007/0-306-47508-1_1

[5] Berkeley. (n.d.). *ELECTROCHEMICAL STUDIES IN CYCLIC ESTERS*.

[6] Deng, D. (2015). Li-ion batteries: Basics, progress, and challenges. In *Energy Science and Engineering* (Vol. 3, Issue 5, pp. 385–418). John Wiley and Sons Ltd. https://doi.org/10.1002/ese3.95

[7] Beard, K. W., & Reddy, T. B. (n.d.). *LINDEN'S HANDBOOK OF BATTERIES, Fifth Edition*.

[8] Buchmann Isidor. (n.d.). *"Batteries in a Portable World - A Handbook on Rechargeable Batteries for Non-Engineers."*

[9] Huang, X. (2011). Separator technologies for lithium-ion batteries. *Journal of Solid State Electrochemistry*, *15*(4), 649–662. https://doi.org/10.1007/s10008-010-1264-9

[10] Marom, R., Amalraj, S. F., Leifer, N., Jacob, D., & Aurbach, D. (2011). A review of advanced and practical lithium battery materials. *J. Mater. Chem.*, *21*(27), 9938–9954. https://doi.org/10.1039/C0JM04225K

[11] Ko, J. M., Min, B. G., Kim, D.-W., Ryu, K. S., Kim, K. M., Lee, Y. G., & Chang, S. H. (2004). Thin-film type Li-ion battery, using a polyethylene separator grafted with glycidyl methacrylate. *Electrochimica Acta*, *50*(2), 367–370. https://doi.org/https://doi.org/10.1016/j.electacta.2004.01.127

[12] Scrosati, B. (2000). Recent advances in lithium ion battery materials. *Electrochimica Acta*, *45*(15), 2461–2466. https://doi.org/https://doi.org/10.1016/S0013-4686(00)00333-9

[13] Suo, L., Hu, Y.-S., Li, H., Armand, M., & Chen, L. (2013). A new class of Solvent-in-Salt electrolyte for high-energy rechargeable metallic lithium batteries. *Nature Communications*, *4*(1), 1481. https://doi.org/10.1038/ncomms2513

[14] Silva, F. A. (2016). Lithium-Ion Batteries: Fundamentals and Applications [Book News]. *IEEE Industrial Electronics Magazine*, *10*(1), 58–59. https://doi.org/10.1109/mie.2016.2515040

[15] Chawla, N., Bharti, N., & Singh, S. (2019). Recent Advances in Non-Flammable Electrolytes for Safer Lithium-Ion Batteries. *Batteries*, *5*. https://doi.org/10.3390/batteries5010019

[16] Chen, M., Zhou, D., Chen, X., Zhang, W., Liu, J., Yuen, R., & Wang, J. (2015). Investigation on the thermal hazards of 18650 lithium ion batteries by fire calorimeter. *Journal of Thermal Analysis and Calorimetry*, *122*(2), 755–763. https://doi.org/10.1007/s10973-015-4751-5

[17] Ren, D., Feng, X., Lu, L., He, X., & Ouyang, M. (2019). Overcharge behaviors and failure mechanism of lithium-ion batteries under different test conditions. *Applied Energy*, *250*, 323–332. https://doi.org/10.1016/j.apenergy.2019.05.015

[18] Feng, X., Ouyang, M., Liu, X., Lu, L., Xia, Y., & He, X. (2018). Thermal runaway mechanism of lithium ion battery for electric vehicles: A review. In *Energy Storage Materials* (Vol. 10, pp. 246–267). Elsevier B.V. https://doi.org/10.1016/j.ensm.2017.05.013

[19] Jiang, Z. Y., Li, H. B., Qu, Z. G., & Zhang, J. F. (2022). Recent progress in lithium-ion battery thermal management for a wide range of temperature and abuse conditions. In *International Journal of Hydrogen Energy* (Vol. 47, Issue 15, pp. 9428–9459). Elsevier Ltd. https://doi.org/10.1016/j.ijhydene.2022.01.008

[20] Jindal, P., & Bhattacharya, J. (2019). Review—Understanding the Thermal Runaway Behavior of Li-Ion Batteries through Experimental Techniques. *Journal of The Electrochemical Society*, *166*(10), A2165. https://doi.org/10.1149/2.1381910jes

[21] Feng, X., Ouyang, M., Liu, X., Lu, L., Xia, Y., & He, X. (2018). Thermal runaway mechanism of lithium ion battery for electric vehicles: A review. *Energy Storage Materials*, *10*, 246–267. https://doi.org/https://doi.org/10.1016/j.ensm.2017.05.013

[22] Golubkov, A. W., Fuchs, D., Wagner, J., Wiltsche, H., Stangl, C., Fauler, G., Voitic, G., Thaler, A., & Hacker, V. (2014). Thermal-runaway experiments on consumer Li-ion batteries with metal-oxide and olivin-type cathodes. *RSC Advances*, *4*(7), 3633–3642. https://doi.org/10.1039/c3ra45748f

[23] Wang, Z., Xiang, H., Wang, L., Xia, R., Nie, S., Chen, C., & Wang, H. (2018). A paper-supported inorganic composite separator for high-safety lithium-ion batteries. *Journal of Membrane Science*, *553*, 10–16. https://doi.org/https://doi.org/10.1016/j.memsci.2018.02.040

[24] Zhang, X., Sun, Q., Zhen, C., Niu, Y., Han, Y., Zeng, G., Chen, D., Feng, C., Chen, N., Lv, W., & He, W. (2021). Recent progress in flame-retardant separators for safe lithium-ion batteries. In *Energy Storage Materials* (Vol. 37, pp. 628–647). Elsevier B.V. https://doi.org/10.1016/j.ensm.2021.02.042

[25] Moon, J., Jeong, J., Kim, J., Kim, S., & Park, J. (2019). An ultrathin inorganic-organic hybrid layer on commercial polymer separators for advanced lithium-ion batteries. *Journal of Power Sources*, *416*, 89–94. https://doi.org/10.1016/j.jpowsour.2019.01.075

[26] Shi, C., Dai, J., Shen, X., Peng, L., Li, C., Wang, X., Zhang, P., & Zhao, J. (2016). A high-temperature stable ceramic-coated separator prepared with polyimide binder/Al2O3 particles for lithium-ion batteries. *Journal of Membrane Science*, *517*, 91–99. https://doi.org/https://doi.org/10.1016/j.memsci.2016.06.035

[27] Feng, G., Li, Z., Mi, L., Zheng, J., Feng, X., & Chen, W. (2018). Polypropylene/hydrophobic-silica-aerogel-composite separator induced enhanced safety and low polarization for lithium-ion batteries. *Journal of Power Sources*, *376*, 177–183. https://doi.org/https://doi.org/10.1016/j.jpowsour.2017.11.086

[28] Nunes-Pereira, J., Kundu, M., Gören, A., Silva, M. M., Costa, C. M., Liu, L., & Lanceros-Méndez, S. (2016). Optimization of filler type within poly(vinylidene fluoride-co-trifluoroethylene) composite separator membranes for improved lithium-ion battery performance. *Composites Part B: Engineering*, *96*, 94–102. https://doi.org/https://doi.org/10.1016/j.compositesb.2016.04.041

[29] Xiang, H., Chen, J., Li, Z., & Wang, H. (2011). An inorganic membrane as a separator for lithium-ion battery. *Journal of Power Sources*, *196*(20), 8651–8655. https://doi.org/10.1016/j.jpowsour.2011.06.055

[30] Parikh, D., Jafta, C. J., Thapaliya, B., Sharma, J., Iii, H. M. M., Silkowski, C., & Li, J. (2021). *Al2O3/TiO2 Coated Separators: Roll-to-roll processing and implications for improved battery safety and performance*.

[31] Rafiz, K., & Lin, J. Y. S. (2020). Safe Li-ion batteries enabled by completely inorganic electrode-coated silicalite separators. *Sustainable Energy and Fuels*, *4*(11), 5783–5794. https://doi.org/10.1039/d0se01058h

[32] Rafiz, K., Lin, J., Arunachala, C. M., Kannan, M., Deng, S., & Green, M. (2021). *Electrode-Coated Inorganic Separators for High Performance and Safe Lithium-Ion and Lithium-Metal Batteries*.

[33] Murali, D. R. L., Banihashemi, F., & Lin, J. Y. S. (2023). Zeolite membrane separators for fire-safe Li-ion batteries – Effects of crystal shape and membrane pore structure. *Journal of Membrane Science*, *680*. https://doi.org/10.1016/j.memsci.2023.121743

[34] Dai, W., Kouvatas, C., Tai, W., Wu, G., Guan, N., Li, L., & Valtchev, V. (2021). Platelike MFI Crystals with Controlled Crystal Faces Aspect Ratio. *Journal of the American Chemical Society*, *143*(4), 1993–2004. https://doi.org/10.1021/jacs.0c11784

[35] Wang, M.-Y., Han, S.-H., Chao, Z.-S., Li, S.-Y., Tan, B., Lai, J.-X., Guo, Z.-Y., Wei, X.-L., Jin, H.-G., Luo, W.-B., Yi, W.-J., & Fan, J.-C. (2020). Celgard-supported LiX zeolite membrane as ion-permselective separator in lithium sulfur battery. *Journal of Membrane Science*, *611*, 118386. https://doi.org/https://doi.org/10.1016/j.memsci.2020.118386

[36] Bushuev, Y. G., & Sastre, G. (2010). Feasibility of pure silica zeolites. *Journal of Physical Chemistry C*, *114*(45), 19157–19168. https://doi.org/10.1021/jp107296e

[37] Banihashemi, F., Ibrahim, A. F. M., Babaluo, A. A., & Lin, J. Y. S. (2019). Template-Free Synthesis of Highly b-Oriented MFI-Type Zeolite Thin Films by Seeded Secondary Growth. *Angewandte Chemie*, *131*(8), 2541–2545. https://doi.org/10.1002/ange.201814248

[38] *FTIR Analysis*. (n.d.). Retrieved October 1, 2023, from https://rtilab.com/techniques/ftir-analysis/#:~:text=What%20is%20FTIR%3F,samples%20and%20observe%20chemical%20properties.

[39] Lv, Y.-K. (2004). An Imprinted Organic-Inorganic Hybrid Sorbent for Selective Separation of Cadmium from Aqueous Solution. *Analytical Chemistry*, *76*, 453–457. https://doi.org/10.1021/ac0347718

[40] Thahir, R., Wahab, A., la Nafie, N., & Raya, I. (2019). SYNTHESIS OF MESOPOROUS SILICA SBA-15 THROUGH SURFACTANT SET-UP AND HYDROTHERMAL PROCESS. *Rasayan Journal of Chemistry*, *12*, 1117–1126. https://doi.org/10.31788/RJC.2019.1235306

[41] Thahir, R., Wahab, A., la Nafie, N., & Raya, I. (2019). SYNTHESIS OF MESOPOROUS SILICA SBA-15 THROUGH SURFACTANT SET-UP AND HYDROTHERMAL PROCESS. *Rasayan Journal of Chemistry*, *12*, 1117–1126. https://doi.org/10.31788/RJC.2019.1235306

[42] Wang, J., Ge, B., Li, H., Yang, M., Wang, J., Liu, D., Fernandez, C., Chen, X., & Peng, Q. (2021). Challenges and progresses of lithium-metal batteries. *Chemical Engineering Journal*, *420*, 129739. https://doi.org/https://doi.org/10.1016/j.cej.2021.129739

[43] Rafiz, K., Harika, N. R. D., & Lin, J. Y. S. (2023). Electrode-supported high-tortuosity zeolite separator enabling fast-charging and dendrite-free lithium-ion/metal batteries. *Electrochimica Acta*, *468*, 143129. https://doi.org/https://doi.org/10.1016/j.electacta.2023.143129

[44] Banihashemi, F., Ibrahim, A. F. M., Babaluo, A. A., & Lin, J. Y. S. (2019). Template-Free Synthesis of Highly b-Oriented MFI-Type Zeolite Thin Films by Seeded Secondary Growth. *Angewandte Chemie*, *131*(8), 2541–2545. https://doi.org/10.1002/ange.201814248

# APPENDIX A

# PREPARATION OF LAB-SCALE ZEOLITE

1. 10 grams of tetraethyl orthosilicate (98% reagent grade from Sigma Aldrich), 12 grams of tetrapropylammonium hydroxide (1.0M in H2O from Sigma Aldrich) and 202 grams of deionized water are mixed in a 500 ml glass beaker. A translucent solution is formed.
2. A clean magnetic stirrer is dropped into the solution in the beaker and the beaker is covered with paraffin wax film. It is then placed on a hot plate that can stir the solution using magnetic stirrer.
3. The solution is stirred at 27 ℃ with an rpm of 600 for 24 hours.
4. Remove the beaker from the hot plate and switch off the hot plate. After 24 hours of stirring, we get a clear and transparent solution. Now, carefully transfer this solution into two 100 ml autoclaves.
5. Place the autoclaves inside an oven which is preheated to 130 ℃ for 8 hours. Place a caution sign indicating high temperature around the autoclaves or oven.
6. Now remove the autoclaves from oven using proper PPE and let them cool down to room temperature. Once they are cooled, drain the mother liquor, and recover the silicalite powder at the bottom of the autoclave by dissolving it in de-ionized water.
7. Transfer this solution into a centrifuge tube and centrifugation is done at 10000 rpm for 20 mins. After centrifugation, the water is drained, and powder is again washed with DI water and centrifugation is done. This process of washing and centrifugation is done for at least three time.

8. After third time of centrifugation, the water is drained, and powder is washed with DI water. The entire solution is taken in a 50 ml beaker for drying at 100 ℃ overnight.
9. The drying process evaporates water, and leaves powder inside the beaker. Now this powder is scrapped using a spatula and grounded well using motor, pestle. Subsequently, the powder is transferred into an alumina crucible for calcination. The powder is calcined in a furnace at 600 ℃ for 10 hours with atmospheric air as the medium. Later, the powder is stored under vacuum conditions.

# APPENDIX B

## SYNTHESIS OF PLATE SILICALITE UNDER STAGNANT CONDITIONS

1. 10 grams of tetraethyl orthosilicate (98% reagent grade from Sigma Aldrich), 4 grams of tetrapropylammonium hydroxide (1.0M in H2O from Sigma Aldrich) and 170 grams of deionized water are mixed in a 500 ml glass beaker. A translucent solution is formed.
2. A clean magnetic stirrer is dropped into the solution in the beaker and the beaker is covered with paraffin wax film to avoid any losses by evaporation. It is then placed on a hot plate that can stir the solution using magnetic stirrer.
3. The solution is stirred at 27 ℃, 600 rpm for 24 hours.
4. Remove the beaker from the hot plate and switch off the hot plate. After 24 hours of stirring, we get a clear and transparent solution. Now, carefully transfer this solution into two 100 ml autoclaves.
5. Place the autoclaves inside an oven which is preheated to 155 ℃ for 10 hours. Place a caution sign indicating high temperature around the autoclaves or oven.
6. Now remove the autoclaves from oven using proper PPE and let them cool down to room temperature. Once they are cooled, drain the mother liquor, and recover silicalite powder at the bottom of the autoclave by dissolving it in de-ionized water.
7. Transfer this solution into a centrifuge tube and centrifugation is done at 10000 rpm for 20 mins. After centrifugation, the water is drained, and powder is again washed with DI water and centrifugation is done. This process of washing and centrifugation is done for at least three time.

8. After third time of centrifugation, the water is drained, and powder is washed with DI water. The entire solution is taken in a 50 ml beaker for drying at 100 ℃ overnight.
9. The drying process evaporates water, and leaves powder inside the beaker. Now this powder is scrapped using a spatula and grounded well using motor, pestle. Subsequently, the powder is transferred into an alumina crucible for calcination. The powder is calcined in a furnace at 600 ℃ for 18 hours with atmospheric air as the medium. Later, the powder is stored under vacuum conditions.

# APPENDIX C

## SYNTHESIS OF PLATE SILICALITE UNDER STIRRING CONDITIONS

1. 4.166 grams of tetraethyl orthosilicate (98% reagent grade from Sigma Aldrich), 3.036 grams of tetrapropylammonium hydroxide (1.0M in H2O from Sigma Aldrich) and 34.833 grams of deionized water are mixed in an 80 ml glass beaker. A translucent solution is formed.
2. A clean magnetic stirrer is dropped into the solution in the beaker and the beaker is covered with paraffin wax film to avoid any losses by evaporation. It is then placed on a hot plate that can stir the solution using a magnetic stirrer.
3. The solution is stirred at 27 ℃, 550 rpm for 24 hours.
4. Remove the beaker from the hot plate and switch off the hot plate. After 24 hours of stirring, we get a clear and transparent solution. The solution is aged for an additional 48 hours without disturbing the solution in the beaker.
5. Now, carefully transfer this solution into two 50 ml autoclaves. It is important to make sure that both the autoclaves weigh equal to have uninterrupted and smooth stirring. Place these autoclaves inside the rotary ball mill oven (from MTI) at desired temperature and required duration. Place a caution sign indicating high temperature around the autoclaves or oven.
6. Now remove the autoclaves from the oven using proper PPE and let them cool down to room temperature. Once they are cooled, drain the mother liquor, and recover silicalite powder at the bottom of the autoclave by dissolving it in de-ionized water.
7. Transfer this solution into a centrifuge tube and centrifugation is done at 10000 rpm for 20 mins. After centrifugation, the water is drained, and powder is again washed

with DI water and centrifugation is done. This process of washing and centrifugation is done for at least three time.

8. After third time of centrifugation, the water is drained, and powder is washed with DI water. The entire solution is taken in a 50 ml beaker for drying at 70 ℃ overnight.
9. The drying process evaporates water, and leaves powder inside the beaker. Now this powder is scrapped using a spatula and grounded well using motor, pestle. Subsequently, the powder is transferred into an alumina crucible for calcination. The powder is calcined in a furnace at 650 ℃ for 8 hours with atmospheric air as the medium. Later, the powder is stored under vacuum conditions.

# APPENDIX D

## PREPARATION OF SLURRY AND COATING THE SEPARATOR

1. To prepare the slurry of zeolite powders, an organic binder is used. It is 5 wt% Polyvinyl alcohol (PVA) aqueous solution.
2. To make 5 wt% PVA aqueous solution, 95 grams of DI water is taken in a conical flask and 5 grams of PVA is added to it while stirring. The stirring is continued for 24 hours till a clear solution is obtained.
3. Now, to prepare a slurry, along with zeolite powder, 5 wt% PVA aqueous solution and DI water are used. The composition of the zeolite slurries is mentioned below:
4. Commercial zeolite: 2.5 grams off zeolite, 0.5 grams of PVA aqueous solution and 2 grams of DI water.
5. Lab-scale zeolite: 1 gram of silicalite, 1 gram of PVA aqueous solution and 0.5 grams of DI water.
6. The slurry is made by mixing the zeolite with binder and solvent in a beaker and manually stirred using a glass rod for about ten minutes to achieve a consistent bubble free slurry.
7. A small piece of cathode is taken (about 4inch*4 inch) and placed on a flat glass surface by clamping it to ensure that it does not move.
8. Now, the doctor's blade calipers height is adjusted according to the thickness of coating required. The thickness should be measured from the flat glass surface. For example: The thickness of the cathode is 60 µm and we need a 45 µm thick zeolite coating on it. Hence, we have to raise the height of the calipers to 105 µm from glass surface and lock it.

9. Once the doctor's blade is adjusted, pour the prepared slurry on the edge of the cathode, and use the doctor blade to pull the slurry along the cathode uniformly.
10. The speed of the doctor blade is different for different zeolites. For commercial zeolite, it should be moved fast around 0.25 cm/sec while lab-scale zeolite needs a speed of 0.5 cm/sec to get a good coating.
11. The coated cathodes are dried in humid chamber at 60% relative humidity and 40 ℃ for 8 hrs.
12. Then, the electrode coated separators are cut into 16mm circles using the cutting machine from MTI. The circular separators are subsequently dried in a vacuum chamber at 70 ℃ for 12 hrs.
13. The activated cathode coated separators are transferred into the glove box carefully for making coin cells.

# APPENDIX E

# CONSTRUCTION OF COIN CELLS

1. For coin cell assembly, CR2032 cases are used that are procured from X2 Labwares, Singapore.
2. There are four main components in a coin cell other than electrodes, electrolyte, and separator. They are bottom case, stainless steel spacers, spring, and top case.
3. Initially a bottom case is taken. Then, a stainless steel spacer is placed in it followed by separator coated cathode.
4. Now, 120 µL of electrolyte (1.0 M $LiPF_6$ in EC/DEC/DEM (1:1:1 v/v/v)) is measured and dropped onto the separator. Then, the anode is placed on the top of separator with carbon surface facing the separator.
5. On the top of anode, a stainless steel spacer and spring are set, and the coin cell is sealed using the top case.
6. The coin cell assembly is turned upside down and crimped using a crimping machine from MTI at 400 psi pressure.
7. After crimping, excess electrolyte comes out of the coin cell and it should be cleaned properly to avoid any kind of safety issues.

# APPENDIX F

## CC-CV TESTING OF COIN CELLS

1. The coin cells made are tested for their charge and discharge characteristics under CC-CV method using the battery testing system (from Neware technologies). The coin cells are placed between the positive and negative terminals of the battery testing system and cycled.
2. After placing the cells in testing terminals, we need to make a program that helps the coin cell to cycle. A desktop is connected to the battery testing system and all the terminals are visible on the desktop. To start the program right click on the terminal where the coin cell is mounted. Then a new window opens asking for various parameters.
3. We need to first decide at what C-rate we have to run the coin cell. I have all my coin cell cycled at lower C-rates to gain more insights on their charge and discharge characteristics.
4. The coin cells are cycled from 3 to 4.2 V at 0.1 C-rate. Also, calculate the active material mass based on the mass loading of the cathode and input the value in the program box.
5. Save the changes made and click start to begin the cell testing.
6. Once the testing is done we can see the data generated by right clicking on the channel and choosing the “view data” option.
7. To save the data, select the export tab, enter the file name, and click on export.
8. The file can then be viewed in the folder we saved.
9. To remove the cell from testing terminal, first stop the testing and then remove it.
10. To stop the testing, right click on terminal and choose the option of “single stop.”

# APPENDIX G

## ELCTROCHEMICAL IMPEDANCE SPECTROSCOPY OF COIN CELLS

1. To measure the impedance of coin cell, connect the positive terminal to sensor and working electrode while the negative terminal to counter electrode and reference electrode.
2. On the desktop, open powersuite application.
3. Go to Tools→Database Management→create new data base.
4. Once new database is created, the experiment can be performed as follows
5. Go to Experiment→New→Browse→open created database
6. Select Power sine→single sine→default SS→enter name of the file(it cannot be same as the name of the database).
7. Click next→no change in "Cell Definitions"→next→no change in "Prescan Definition"→next→"Scan Definition."
8. In Scan Definition section, input the values of start frequency, end frequency and points per decade. The start frequency is 100 KHz and the end frequency is 1.5 Hz while select points per decade = 5 and the rest remains unchanged.
9. Click next→no change in "Advanced" →Finish.
10. Then, a new test run window appears where voltage and current values are shown. Make sure that the voltage is positive otherwise recheck the connections of positive and negative terminals.
11. As the experiment start, Nyquist plots are of our main concern.
12. At the end of the test run, right click on the graph and select "Export Data" which gives us all the data points in a text file that can be saved on the desktop.

# APPENDIX H

## OPERATION OF GLOVE BOX AND ITS MAINTENANCE

## A1. OPERATION OF GLOVE BOX

1. All the cathode, anode and electrolyte materials need to be stored inside the glove box as they oxidize when they come in contact with atmospheric air.
2. To transfer the materials in and out of the glove box, antechambers are used. Usually, small antechamber is utilized to take cathode, anode, and electrolyte materials. However, to take some large equipment such as hot plate, crimping machine, large ante chamber is used
3. The ante chambers are always stored under vacuum. In order to open the antechamber, first fill it with the working gas (UHP Argon).
4. Then, load the required samples into it that are meant to be inside the glove box and close the door. Since the antechamber is exposed to the atmospheric air, to avoid that air entering the glove box, the chamber is evacuated and refilled with working gas for at least three times. During this process, the pump should be on.
5. Now, wear proper nitrile hand gloves and put the hands into the glove box. Open the ante chamber door inside the glove box and take the materials into the glove box.
6. After the construction of coin cells, load them into the antechamber and bring them out for testing. Make sure to tightly close the door of antechamber to avoid any seepage of atmospheric air into the glove box.
7. Remove the hands from glove box and open the door of ante chamber outside the glove box to get out the coin cell samples. After removing the samples, properly

seal the antechamber and evacuate, refill the chamber for three times and finally leave the chamber under vacuum.

## A2. REGENERATION OF CATALYST BED

1. The oxygen and moisture content of the glovebox ideally should be at 0.1 ppm. This is maintained by the catalyst bed column connected to the glovebox. However, after some time the catalyst needs to be regenerated to hold back the water and moisture content effectively.
2. Thus, it is highly recommended to regenerate the catalyst bed for every three months. Before beginning the regeneration process, make sure that regeneration gas cylinder is connected to the glove box, and it is completely filled.
3. The outlet flow rate of the regeneration gas should be adjusted to 20 mm. It is important to note that once regeneration process is started, it cannot be aborted for any reason.
4. To begin regeneration, click “REGEN” switch provided on the control panel located on the top right edge of the glovebox.
5. Then the display will ask “Hand Valves open?.” Press down and hold, the right arrow switch to toggle display from “OPEN” to “CLOSED” and press “ENTER” key to confirm the setting.
6. The display will then ask, “Is Flow Ok?.” The display read the answer as “NO.” To switch the answer to “YES,” press down and hold, the right arrow to toggle the display and press “ENTER” to confirm the command.

7. Then the blower switch will be turned off automatically and regeneration of column starts. The cycle lasts for 870 mins in total and cannot be aborted after 10 mins of initiation. After the regeneration, turn off the regeneration gas supply and switch on the blower.